Innovative (electro-driven) sample preparation tools for metabolomics study of muscle aging

He, Y.

Chapter 4

A fully automated and high-throughput three-phase electro-extraction setup hyphenated to LC-MS analysis

Based on:

Yupeng He, Paul Miggiels, Nicolas Drouin, Peter W. Lindenburg, Bert Wouters, Thomas Hankemeier

An automated online three-phase electro-extraction setup with machine vision process monitoring hyphenated to LC-MS analysis

Analytica Chimica Acta (2022)

Yupeng He, Paul Miggiels, Nicolas Drouin, Amy Harms, Bert Wouters, Thomas Hankemeier

A novel technology for sample preparation: A fully automated, high-throughput and online electro-extraction platform

In preparation

ABSTRACT

Sample preparation is a labor-intensive and time-consuming procedure, especially for the bioanalysis of large numbers of samples with small volume/mass and low concentration analytes. To address these analytical challenges, strategies have to be considered to enrich the molecules of interest which allow for high-throughput analysis. Three-phase electro-extraction (EE) is an emerging sample-preparation method especially suited for the enrichment of low concentration and small volume samples. However, this method is still lacking full automation and hyphenation to LC-MS, and the stability and performance of automated EE have to be evaluated before its application to biological samples.

For this study, two modules for three-phase EE were developed, integrated on a CTC PAL robotic autosampler hyphenated to LC-MS. In phase 1, a 3-well plate EE module with machine vision was used for the initial optimization and evaluation of automated EE using eight model compounds, *i.e.*, amitriptyline, clemastine, clomipramine, haloperidol, loperamide, propranolol, oxeladin, and verapamil. The stability of the EE was evaluated by monitoring the droplet size by machine vision and recording the current during EE. Three crucial EE parameters, *i.e.*, the ratio of formic acid in the sample to acceptor phase, extraction voltage, and time were thoroughly optimized by a Design of Experiment approach (Box-Behnken design). Electroextraction could be achieved in less than 2 min with enrichment factors (EF) up to 387 and extraction recoveries (ER) up to 97% for academic samples with a stable method. The optimized EE method was then successfully applied to both spiked human urine and plasma samples with low-concentration (50 ng mL^{-1}) analytes and a low sample volume (20 µL starting volume of plasma and urine in 10-fold diluted samples) for bioanalysis evaluation. A stable and high enrichment automated EE setup was obtained during the evaluation of this first module. However, the designed well plate of this first EE module could hold only three samples. For the start of each new sample, the well plate had to be manually moved to the proper position to align the syringe needle with the sample, which does not provide the required throughput for bioanalysis. Therefore, a second module for fully automated and high-throughput EE as developed to address these shortcomings in phase 2. An in-house-developed 96-well plate with an integrated bottom electrode was utilized for the analysis of acylcarnitines in *Ercc1*$^{\Delta/-}$ mice muscle tissue for a sarcopenia study. Acylcarnitines play important roles in fatty acid transport, β-oxidation, and energy production in muscle cells, which are highly related to muscle function and

sarcopenia. Ten kinds of representative acylcarnitines were utilized as model analytes for the setup optimization. The optimal EF was up to 397, and the ER was up to 99% in academic samples. The optimal method was characterized using spiked human plasma samples from an equivalent of 20 µL plasma and was also utilized for the study of muscle tissue isolation speed effects on acylcarnitines stability in progeroid (*Ercc1*$^{\Delta/-}$) mice muscle. We found that muscle isolation speed (fast or 15-min delayed isolation at room temperature) does not affect measured levels of acylcarnitines from tissue samples.

This study supplies a solution for high-throughput sample preparation for large numbers of samples with limited quantity and provides a direction for the development of fully-automated bioanalysis workflows in the future.

1. Introduction

Sample preparation poses a significant bottleneck in bioanalysis workflows for large numbers of samples, especially for biomass-limited samples, *i.e.*, samples that are low in mass/volume and/or have a low concentration of analytes [1-4]. One example of a biomass-limited use-case is muscle tissue from mice deficient in the DNA excision-repair gene *Ercc1* (*Ercc1*$^{\Delta/-}$), which show numerous age-related pathologies and accelerated aging features [5-8], such as sarcopenia [9-12]. Moreover, these progeroid mouse mutants (*Ercc1*$^{\Delta/-}$) and the corresponding human DNA repair syndromes are severely growth-retarded as the consequence of attenuation of the IGF1/growth-hormone somatotrophic axes [13-15], limiting sample size for analysis. Manual sample preparation is laborious and often time-consuming, which negatively impacts its repeatability [16-19]. Alternative strategies must be pursued to achieve consistent extraction performance and high throughput. This has been a driving force for the development of fully-automated sample-preparation techniques that can clean up and preconcentrate analytes, can consistently handle small volumes/mass, minimize solvent consumption, and can be directly coupled to analytical instrumentation such as liquid chromatography-mass spectrometry (LC-MS) or capillary electrophoresis – mass spectrometry to minimize sample loss [1, 16, 20-25].

Liquid-liquid extraction (LLE) and solid-phase extraction (SPE) are the most commonly used sample-preparation techniques [26-28]. However, both are labor- and time-consuming and use relatively large amounts of environmentally unfriendly organic solvents, which in turn also results in the dilution of the analytes for small-volume samples. Electro-driven techniques are emerging sample-preparation methods as they offer a simple extraction process that achieves simultaneous clean-up and high enrichment from biomass-limited samples [29-32]. Electro-driven extraction techniques can be categorized as supported liquid membrane electro-membrane-extraction (SLM-EME) and free liquid membrane electro-membrane-extraction (FLM-EME), with the main difference being the presence of a solid membrane between the sample and acceptor [32]. Due to the absence of the solid membrane, FLM-EME is more straightforward in design, costs, and potential for automation. Three-phase electro-extraction (EE) is a subtype of FLM-EME, with an aqueous acceptor droplet formed in the organic phase and was first reported by Raterink *et al.* in 2013 [33]. Most electro-driven extraction methods reported so far have been manually operated with little potential for automation [33-41]. Raterink *et al*. performed three-phase

EE on an automated nanoESI robot (Triversa NanoMate) that allowed for direct coupling to the mass spectrometer. However, this system could only be hyphenated offline to separation instruments, which would lead to the injection of a fraction of the extract. [33]. The CTC PAL robotic autosampler is an established auto-sampler platform that provides flexibility for the integration of in-house developed setups and hyphenation to LC. Therefore, it could be an ideal platform to achieve both automation and high-throughput analysis for the three-phase EE method. A digital camera was widely used in three-phase EE to monitor the acceptor droplet status [25, 33, 36, 41]. However, the stability of the droplet during EE and the effect of this stability on EE are so far still unclear. The current during EE was also reported to monitor EE status [42], but its relation to EE performance still needs to be further investigated. Therefore, an EE setup integrated into a robotic autosampler with machine vision for acceptor droplet volume calculation and current monitoring is a promising method to optimize the three-phase EE method.

During the first phase of this study, we developed an automated on-line three-phase EE module with a 3-well plate integrated on a CTC PAL robotic autosampler, equipped with machine vision and current monitoring. Eight commonly-used model compounds, namely amitriptyline, clemastine, clomipramine, haloperidol, loperamide, propranolol, oxeladin, and verapamil were utilized for this stability evaluation and three-phase EE performance estimation [35, 36, 43]. During the second phase of the study, the three-phase EE module was upgraded to a fully automated and high-throughput sample preparation setup by using an in-house developed 96-well plate for the analysis of acylcarnitines in human plasma and in muscle tissue from *Ercc1*$^{\Delta/-}$ mice, which play important roles in fatty acid transport from the cytoplasm into mitochondria for β-oxidation and energy production in muscle cells and which are highly associated with muscle function and sarcopenia. Raterink *et al*. optimized parameters for the electroextraction of acylcarnitines in their manual EE method [33]. Three crucial EE parameters, *i.e*., the ratio of formic acid (FA) in the sample to acceptor phase, extraction voltage, and extraction time, and ten representative acylcarnitines, *i.e*., carnitine, acetyl-carnitine, propionyl-carnitine, isobutyryl-carnitine, valeryl-carnitine, hexanoyl-carnitine, octenoyl-carnitine, octanoyl-carnitine, decanoyl-carnitine, and lauroyl-carnitine, were utilized for the setup optimization. The optimal method for acylcarnitines was first evaluated using human plasma samples and the utility was then demonstrated on *Ercc1*$^{\Delta/-}$

mice muscle tissues to investigate whether fast sample isolation (after mouse dissection) is necessary for acylcarnitine stability.

2. Material and methods

2.1. Chemicals

Amitriptyline, clemastine, clomipramine, haloperidol, loperamide, propranolol, oxeladin, verapamil, L-carnitine, acetyl-L-carnitine, DL-decanoylcarnitine, DL-hexanoylcarnitine, lauroyl-L-carnitine, isobutyryl-L-carnitine, DL-octanoylcarnitine, octenoyl-L-carnitine, propionyl-L-carnitine, valeryl-L-carnitine, and crystal violet were all purchased from Sigma-Aldrich (Steinheim, Germany). MilliQ water was obtained from a Millipore high-purity water dispenser (Billerica, MA, USA). Formic acid and acetic acid were purchased from Acros Organics BVBA (Geel, Belgium). Ethyl acetate and acetonitrile were purchased from Biosolve Chimime SARL (Dieuze, France). All solvents were HPLC grade or higher.

2.2. Standard and sample solutions

Stock solutions of all model compounds (amitriptyline, clemastine, clomipramine, haloperidol, loperamide, propranolol, oxeladin, and verapamil) were prepared in 1:1 MeOH: H_2O (v/v) in 100 μg mL^{-1} and stored in 4°C. Prior to analysis, academic samples were prepared by diluting stock solutions to a concentration of 500 ng mL^{-1} in the desired percentage of formic acid (FA) in MilliQ water. To evaluate the method in human plasma and urine samples, 50 ng mL^{-1} of amitriptyline, clemastine, clomipramine, haloperidol, loperamide, propranolol, oxeladin, and verapamil were spiked to undiluted, 5-fold, and 10-fold diluted urine and plasma with and without protein precipitation (PP). Freshly pooled urine samples were obtained from adult, healthy volunteers (age 27 to 32). EDTA-treated plasma samples (obtained from Sanquin, Leiden, the Netherlands) were kept frozen at −80 °C until analysis and were thawed at room temperature only directly before use.

Stock solutions of acylcarnitines (6.25 μg mL^{-1}) were prepared in MeOH. Standard solutions were prepared by diluting stock solutions to a concentration of 200 ng mL^{-1} in a stated percentage of FA as academic samples. Standard solutions were also spiked to undiluted, 5-fold, and 10-fold diluted plasma samples with and without PP in a concentration of 200 ng mL^{-1}, to evaluate the optimized EE method. For PP, ice-cold MeOH was used for the protein precipitation of plasma samples with a ratio MeOH: plasma of 4:1, v/v [44]. The supernatant was evaporated to dryness using a SpeedVac Vacuum

concentrator (Thermo Savant SC210A, Waltham, Massachusetts, United States) and reconstituted at the stated percentage of FA in water to the 1-, 5-, and 10-times dilution with regards to the starting volume.

2.3. Muscle samples

Muscle tissue from mice deficient in the DNA excision-repair gene *Ercc1* (*Ercc1*$^{\Delta/-}$) was utilized for the study of the effect of sample isolation speed on acylcarnitine stability. The generation and characterization of *Ercc1*$^{\Delta/-}$ mice are described in [6, 7, 12]. The three most commonly used mouse muscle types for molecular analyses, gastrocnemius + soleus (Gas + Sol), quadriceps (Quadr), and extensor digitorum longus + tibialis anterior (EDL + TA), were collected at the animal facility of the Erasmus Medical Centre, Rotterdam, The Netherlands. All above experiments were performed in accordance with the Principles of Laboratory Animal Care and with the guidelines approved by the Dutch Ethical Committee (permit no. 139-12-13, and 139-12-18) in full accordance with European legislation.

Fast and delayed (15-min delayed) muscle tissue collection procedures were applied to study the effects of sample isolation speed on acylcarnitine stability. Briefly, mice were anesthetized using CO_2. For fast sample isolation, first a large piece of Quadr tissue was dissected immediately and rapidly frozen in liquid nitrogen. Then EDL + TA and Gas + Sol tissue were carefully isolated as described in [45] and were immediately frozen in liquid nitrogen-cooled isopentane and stored at -80 ºC [11]. For delayed sample isolation, the Quadr, EDL + TA, and Gas + Sol tissues from the other hind leg of the same mouse were kept 15 min at room temperature, then were isolated and frozen as described above for the fast isolation. All samples were stored at -80 ºC until analysis.

Before the extraction by automated EE, the mouse muscle tissues were firstly lyophilized in a VaCo I freeze-dryer (Zirbus, Bad Grund, Germany; connected to an E2M12 high vacuum pump, Edwards, Crawley, England) for 24 hours and weighed. Dry-homogenization in a Bullet Blender (BBX24; Next Advance, Averill Park, NY, USA) for 15 min at speed 9 with 100 mg (± 10%) zirconium oxide beads (0.5 mm; Next Advance, Averill Park, NY, USA) was conducted to the freeze-dried tissue [46]. 200 µL formic acid solution (with optimum percentage) was added to Eppendorf tubes used for homogenization, then the solvent and muscle were moved to the designed 96-well plate for electroextraction.

2.4. Automated EE setup and extraction process

The fully integrated and automated EE and injection procedures were performed on a CTC PAL3 RSI/RTC dual-headed robotic autosampler (CTC Analytics AG, Zwingen, Switzerland), equipped with a 6-port VICI Cheminert Nanovolume vertical port injector valve with 2-µL stainless steel loop (VICI AG, Schenkon, Switzerland), and two custom modules for the electro-extraction process (Figure 1A).

2.4.1 Phase 1: 3-well plate EE with machine vision and current monitoring

The EE module for droplet stability evaluations (Figure 1B) consisted of a support for a custom 3-well sample holder fitted with a LED backlight and a colour CMOS camera (Basler dart daA1600-60UC; Basler AG, Ahrensburg, Germany) with a 2x zoom, 40-mm working distance telecentric lens (TechSpec® CompactTL™; Edmund Optics Ltd., York, United Kingdom), mounted to two translation stages to adjust the height and distance. To visualize the acceptor droplet, a transparent 3-well sample holder was used, which consisted of four parts that were screw-assembled, described from top to bottom as follows: a 98×16×6 mm piece of cyclic olefin copolymer (COC) in which three oblong through-holes with a volume of 380 µL were CNC milled (Haas OM2-A; Haas Automation Inc. Oxnard, CA, USA), ethylene propylene (EP) O-rings (0.9-mm diameter, 28.3-mm length; Apple Rubber Products Inc., Lancaster, NY, USA) for leak-tight sealing, a 1-mm strip of aluminum as an electrode, and an 8-mm strip of polyetheretherketone (PEEK) for rigidity and electrical insulation. The PEEK strip featured three sockets for a ball-detent locking mechanism for sideways alignment of the wells. COC was chosen for its optical transparency, chemical resistance to the solvents used, and good machinability.

2.4.2 Phase 2: 96-well plate for high-throughput and fully-automated EE

A 2.2 mL polypropylene 96-well plate (Ratiolab, Dreieich, Germany) was modified by cutting off the cone bottom to form a 3-mm diameter circular hole in each well (Figure 1B). An aluminum plate (116 × 74 × 2.4 mm) with 96 protrusions (3.0 mm diameter, 3.4 mm height) was fabricated to be assembled with the modified 96-well plate. Ethylene propylene diene monomer (EPDM) O-rings 3×1 mm (ERIKS, Alkmaar Netherlands) were used for sealing the wells. EPDM O-rings were selected for their chemical resistance to the solvents used and cost-efficiency. Four screws (2.8 mm diameter) and gaskets were used for assembly stability. Nuts fitting the screw size were fabricated in four positions in the corners

of the aluminum plate (Figure 1B). A polyether ether ketone (PEEK) plate (127.4 × 85 × 6 mm) was fabricated and assembled on the bottom of the aluminum plate to insulate the electrode from the autosampler. Two holes in the PEEK plate were used for the power cable connection with the aluminum plate (Figure 1B). All custom parts were designed and manufactured by the Fine Mechanical Department at Leiden University.

2.4.3 Automation

The CTC PAL3 autosampler was programmed and controlled with PAL Sample Control (PSC) 3.10 (CTC Analytics AG, Zwingen, Switzerland). The EE module was integrated into the autosampler as a general injector module with adjustable injection depth, and the depth was fixed after calibration. The extraction process was controlled by a house-developed program created under LabView 2021 (National Instruments, Austin, Texas, USA) program that set the process voltage and timing, recorded the video of the process, and logged the process current to a file at a rate of 10 frames or measurements per second. An NI USB-6008 interface (National Instruments, Austin, Texas, USA) was used to synchronize with the autosampler via start/stop signals, provide 0-5V control signal to the power supply, and monitor the process current. All parameters for the process such as droplet volumes, extraction voltage, and extraction time were entered in the PSC sample list and shared with the LabView program via a plaintext file.

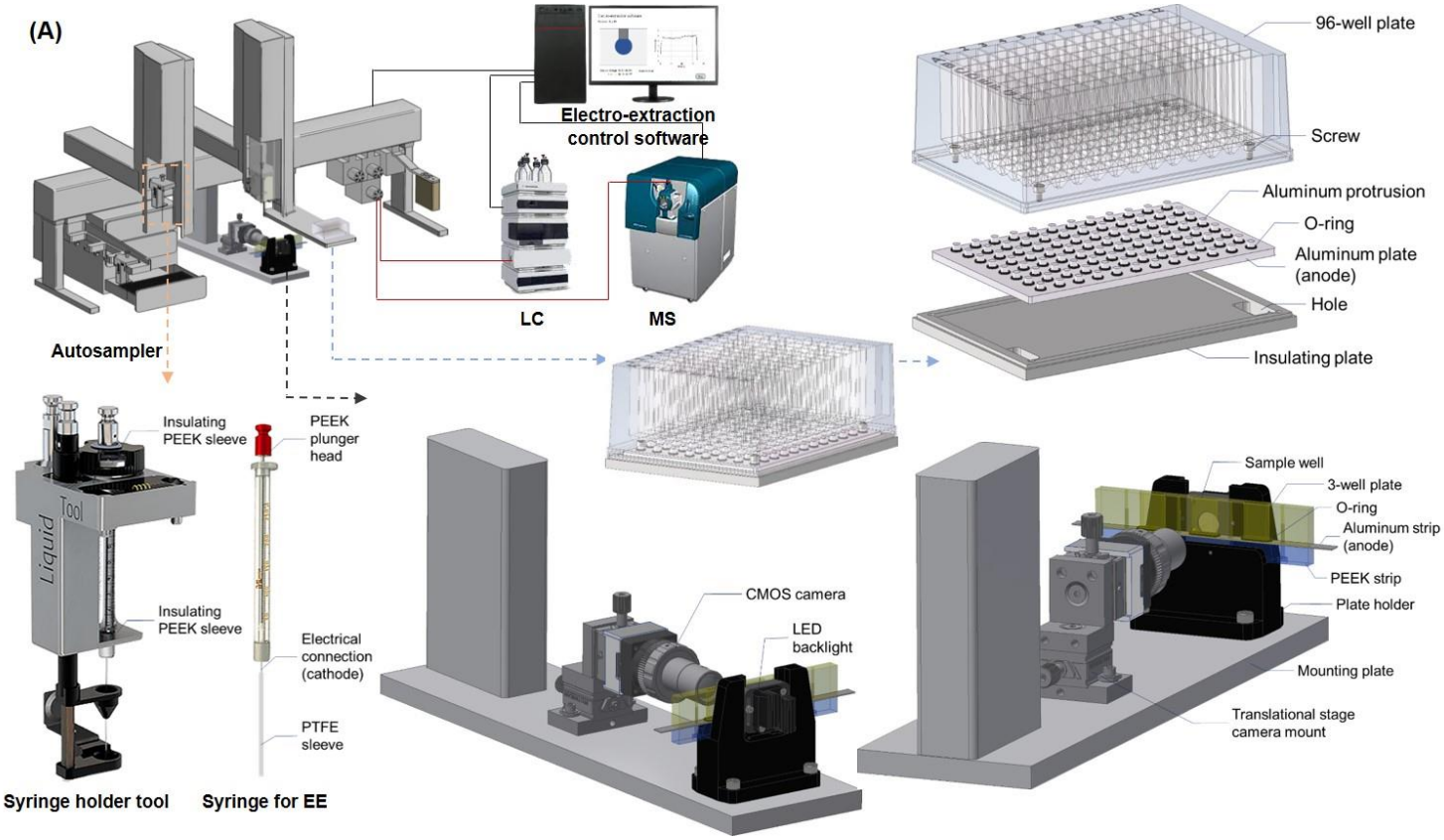

Figure 1. Schematic diagram of the electro-extraction module integrated on the autosampler (A), modified syringe holder tool and syringe for EE (B), details of the EE 3-well plate and imaging setup (C), and the details of the modified 96-well plate with a house-made bottom electrode (D).

2.4.4 The extraction process

The extraction was performed with a 10-µL glass syringe with a G22s needle (CTC Analytics AG, Zwingen, Switzerland) that was fitted with a PEEK plunger head for electrical insulation and a polytetrafluoroethylene (PTFE) sleeve (1/32" ID, 1/16" OD) around the lower part of the needle. Additional custom PEEK sleeves and insets were placed in the syringe tool holder to eliminate potential points of electrical contact between the syringe and the autosampler (Figure 1C). The process voltage was supplied by a 0-1500 V DC high voltage power supply (RB10 1.5P, Matsusada Precision, Shiga, Japan) with an external 0-5 V DC control. Electrical connections were made with insulated clamps, one at the COC wells (anode) and one at the uncovered section of the syringe needle (cathode). Two additional resistors were placed in series with the process: a 10 MΩ current limiting resistor for operator safety, and a 100 kΩ shunt resistor to measure the process current. These values were chosen to minimally affect the process under the assumption that the process resistance exceeded 1 GΩ.

Phase 1: 3-well plate EE with machine vision and current monitoring

The extraction process was as follows: for the evaluation of the acceptor droplet stability by using the EE module with a 3-well plate and machine vision (in 2.4.1), 200 µL of aqueous sample and 100 µL of the organic phase (water-saturated ethyl acetate) were transferred into a well; 6 µL of acceptor phase was aspirated by the modified 10-µL syringe; the syringe needle was lowered into the extraction well and a 0.5 µL acceptor droplet was formed at its tip; the extraction was started at the set voltage and time; the acceptor droplet was aspirated and subsequently injected in the injection valve towards the LC-MS; the 10-µL syringe was then cleaned with MeOH and water 3 times. All samples and solvents were stored at 6 °C in the drawer of the autosampler.

Phase 2: 96-well plate for high-throughput and fully-automated EE

For the optimization and analysis of acylcarnitines in academic and plasma samples by using the high-throughput EE module (in 2.4.2), all the solvents and samples were stored at 6 °C in the drawer of the autosampler. The extraction process was shown in Figure S1. At the start of sample analysis, 200 µL of aqueous sample and 250 µL of MilliQ water-saturated ethyl acetate were transported separately from vials in the drawer to the 96-well plate for electroextraction by using the autosampler left head with a 1000-µL glass syringe

(CTC Analytics AG, Zwingen, GmbH). After transport of each sample/solvent, the 1000-µL syringe was cleaned with MeOH and water, 3 times each. Then EE was applied by a 10-µL syringe on the autosampler right head as described above. This workflow would then repeat itself for the next sample analysis. For muscle tissue extraction, 250 µL of MilliQ water-saturated ethyl acetate was transported to the 96-well plate containing the formic acid homogenized muscle samples by the autosampler left head with a 1000-µL glass syringe. The extraction process was the same as described above.

2.5. LC-MS methods

The autosampler was coupled to an Agilent 1200 Series G1312B pump (Agilent, Waldbronn, Germany) and a Sciex 5600+ Triple-time-of-flight mass spectrometer (TripleTOF/MS; AB Sciex LLC), and a Synergi™ Phenomenex C18 LC column (50×2 mm, 4-µm particle size) kept at 40 °C with an Agilent 1200 Series G1316A column oven (Agilent, Waldbronn, Germany). For both model compounds and acylcarnitines analysis, the LC was used with an isocratic mobile phase composition of 60:40 water:acetonitrile with 0.1% acetic acid and a flow rate of 0.3 mL min^{-1}. The pump was controlled by Lab Advisor version B.02.07 (Agilent, Waldbronn, Germany). Source settings for the mass spectrometry were set as follows: curtain gas 270.96 kPa, source temperature 400 °C, ion source voltage 4.64 kV. Spectral data was acquired in full scan with a range of 100-1000 *m/z* and scan rate of 10 scans/s in positive ionization mode using Sciex Analyst 1.7 (AB Sciex LLC, Framingham, MA, USA). Peaks were extracted with mass accuracy of ± 0.02 width. And integrated with MultiQuant version 3.0.1 (AB Sciex LLC, Framingham, MA, USA).

2.6. Data analysis and calculation

Statistical analysis was conducted with SPSS (IBM Statistics 25). Design-Expert (version 12.0, Stat-Ease, Minneapolis, USA) was utilized for the optimization of the parameters of the three-phase EE by using a Box-Behnken design (BBD) of experiment. The enrichment factor (EF) [30, 33, 36] and extraction recovery (ER) [30, 47] were calculated by Equations 1 and 2:

$$EF = \frac{(Analyte\ peak\ area\ in\ acceptor\ phase)_{after\ EE}}{(Analyte\ peak\ area\ in\ aqueous\ sample)_{before\ EE}} \quad \text{(Equation 1)}$$

$$ER(\%) = EF \times \frac{V_d}{V_s} \cdot 100\% \quad \text{(Equation 2)}$$

where V_d and V_s are the volumes of the acceptor droplet (0.5 mL) and the aqueous sample (200 mL), respectively.

To assess the stability of the droplet volume during extraction, the droplet volume was calculated from the recorded videos with a custom LabView program. Firstly, the needle region was selected for each video and an appropriate binarization threshold was chosen. Then for each frame, the image was binarized, and connected holes in the drop and needle perimeter were filled. Next, the needle region was subtracted, and after hole-filling and particle removal, a binary matrix of the drop profile was obtained (Figure S2). The drop volume can be calculated from this using disc integration along the vertical axis, using the sum of each row as the diameter of the disc: $V_{droplet} = \frac{\pi}{4} d_{px}^3 \sum_{i=1}^{n} \sum_{j=1}^{n} x_{i,j}^2$, in which is d_{px} the known size of a square pixel of 2.25 µm.

For acylcarnitines analysis, the limits of detection (LODs) were calculated by using the method described in [48]. The peak areas of acylcarnitines were normalized by the muscle dry weight and statistically analyzed for the study of muscle isolation speed effect on acylcarnitine stability.

3. Results and discussion

Development of the automated EE setup occurred in two phases. Firstly, the performance of a 3-well plate EE setup was evaluated by the stability of the acceptor droplet size (as calculated by the machine vision system) and the current monitored during the EE procedure. Eight model compounds were utilized, three crucial parameters of the three-phase EE were optimized, and the optimal automated EE method was applied to human plasma and urine samples for the evaluation. Secondly, the parameters of a 96-well plate high-throughput fully-automated EE setup were optimized for simultaneous extraction of ten acylcarnitines in academic samples. The optimal method was then applied to human plasma samples for evaluation and *Ercc1*$^{\Delta/-}$ mice muscle tissues to investigate the effects of tissue isolation speed on acylcarnitine stability.

3.1 Phase 1: Evaluation of the 3-well plate EE setup with machine vision and current monitoring

3.1.1 Evaluation of the setup performance

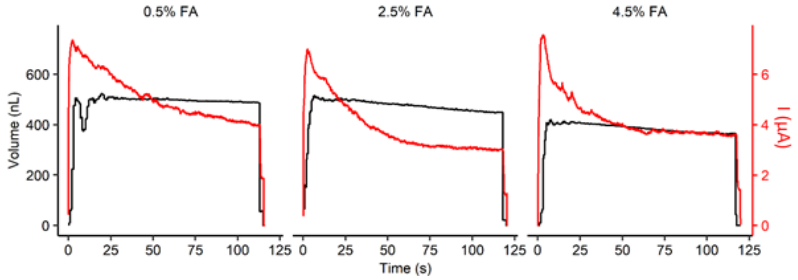

Figure 2. Droplet volume (black color) and process current (red color) during the extraction of crystal violet at 150 V extraction voltage, 120 s extraction time and various percentages of formic acid in the acceptor phase.

The electro-extraction process was firstly evaluated visually by extracting 1 µg mL^{-1} of the cationic dye crystal violet. The acceptor droplet colored dark blue from the extracted dye within seconds after starting the extraction and the droplet remained stable for over 120 seconds. This was repeated for various concentrations of formic acid in samples and the droplet volume and process current were used to assess the stability and progress of the EE process. Figure 2 shows that the acceptor droplet volume remained stable (-40 nL) throughout the extraction process. The slight decrease of the calculated droplet volume may be due to the electrolysis of crystal violet [49].The current declined with extraction time, eventually stabilizing for higher percentages of FA. The current decrease was slower for lower percentages of FA, which supported the theoretical model (Equations 3 and 4) that high fluxes (J_i) and current can be obtained with low ion balances (χ) [42, 43, 50].

$$J_i = \frac{-D_i}{h}\left(1 + \frac{v}{\ln \chi}\right)\left(\frac{\chi - 1}{\chi - \exp(-v)}\right)(C_{ih} - C_{i0}\exp(-v)) \qquad \text{(Equation 3)}$$

In Equation 3, i indicates the ith cationic substance; D_i is the ith ion diffusion coefficient; h is the membrane thickness; C_{ih} and C_{i0} are the concentration of ith cationic substance in the sample solution and the acceptor phase; v is a dimensionless driving force which is related to the applied electrical potential; χ the ion balance, *i.e.*, the ratio of the total ionic concentration in the sample to that in the acceptor phase.

$$I = \sum_i J_i z_i F + \sum_k J_k z_k F \qquad \text{(Equation 4)}$$

In Equation 4, the first term ($\sum_i J_i z_i F$) represents the current (I) carried by cationic substances, and the second term ($\sum_k J_k z_k F$) accounts for the anionic substances. i indicates the ith cationic ion, z_i is the charge of the ith cationic ion; k indicates the kth anionic ion, z_k is the charge of the kth anionic ion, and F is the Faraday constant.

3.1.2 EE optimization for eight model compounds

3.1.2.1. Optimization model design and model quality

The operational EE parameters were optimized to maximize the enrichment factor using a Box-Behnken design (BBD). Based on the theoretical model of the analyte flux (J_i) in Equation 3 [42], the total extraction can be increased by modulating analyte flux (J_i). J_i can be most easily improved by increasing the applied voltage (increasing v) or decreasing the ion balance (χ) by altering the ratio of formic acid in the sample to the acceptor phase [42]. However, there is an antagonist effect between extraction voltage and time, *i.e*., an increase in extraction voltage limits the extraction time and vice versa [36, 50]. Therefore, simultaneous optimization of the process was done with formic acid ratio (A), extraction voltage (B), and extraction time (C) as parameters.

A quadratic model was adopted in BBD, and seventeen experiments were conducted in triplicate with 5 center points. The investigating range for each parameter is listed in Table 1. The maximum voltage was set to 250 V because of the instability of the acceptor droplet at extraction voltages above this value. This maximum was determined as the voltage at which the acceptor droplet was kept stable for at least 120 seconds.

Table 1. Investigated parameters for Box-Behnken design.

Code level	A: FA% or ratio of FA in the sample to acceptor phase (2% FA in acceptor phase)	B: Voltage (V)	C: Extraction time (S)
-1	0.5% (0.25)	50	10
0	2.5% (1.25)	150	65
1	4.5% (2.25)	250	120

Note: Code −1, 0, and 1 were used to represent low, middle, and high levels of parameters.

Table 2 showed that the developed models were significant for all model compounds with $p<0.001$. The lack of fit of these models was not significant with p-values larger than 0.06, demonstrating that the developed models fit well with the parameters utilized for optimization for all compounds. The statistical evaluation of the coefficients also revealed a good fit of the models with R^2 and adjusted R^2 above 0.95 and 0.88, respectively, for all model compounds (Table 2). Overall, the developed models fit well with the experimental values for the subsequent method optimizations.

3.1.2.2 Optimization of the automated EE method

From the models, it followed that the optimal enrichment factors taking all analytes into account could be achieved with a formic acid ratio of 1.65 (3.3% in the sample, 2% in the acceptor phase), extraction voltage of 135 V, and extraction time of 98 s (Figure 3 and S2). When increasing the formic acid percentage from 0.5 to 3.3%, the increase in enrichment factors may be due to the contribution of increased buffer capacity and more stable pH during EE at a high formic acid percentage. However, the EF decreased again above the optimal FA percentage. A similar trend was also observed in our previous study [36]. The decline in the enrichment factor at higher percentage FA may be due to an overly high ion balance (χ) induced by the high cation concentration in the sample solution under these conditions [40, 51].

Higher extraction voltage contributes to faster migration of the charged analytes during electro-extraction and therefore improves the extraction efficiency. However, for voltages over 135 V, the EF of the model compounds decreased (Figure 3 and S3). Similarly, the EF declined again when exceeding the optimal extraction time of 98 s (Figure 3 and S3). Similar results were also reported by Nojavan *et al.*, in their case for extraction voltages and times over 20 V and 15 min [52], and 250 V and 20 min, respectively [53], and by Schoonen *et al.* for an extraction voltage over 300 V [54]. The decrease in enrichment above the optimum voltage and time could be attributed to excessive electrolysis [51, 55-57]. Electrolysis in the cathode acceptor phase increases the pH of the acceptor phase, leading to a neutralization of the charge of the model compounds. This in turn reduces their polarity and increases back-extraction into the organic phase through a passive liquid-liquid extraction mechanism, which has been reported in numerous publications [29, 33, 36, 37, 51, 57]. This was consistent with previous observations that there is an antagonistic effect between extraction time and voltage [36, 50].

Table 2. p-values and R^2 of response surface quadratic models for EF of model compounds.

Source	Amitriptyline	Clemastine	Clomipramine	Haloperidol	Loperamide	Oxeladin	Propranolol	Verapamil
Model	< 0.0001	< 0.0001	0.0004	< 0.0001	0.0009	0.0003	< 0.0001	< 0.0001
A: FA	0.0031	0.0244	0.0571	0.1511	0.0251	0.0835	0.0535	0.0460
B: Voltage	0.4583	< 0.0001	0.0032	< 0.0001	0.0773	0.0152	0.9216	0.0010
C: Time	< 0.0001	< 0.0001	< 0.0001	< 0.0001	< 0.0001	< 0.0001	< 0.0001	< 0.0001
AB	0.1126	0.2022	0.4166	0.3403	0.8572	0.2768	0.0701	0.0317
AC	0.4658	0.1067	0.1441	0.2074	0.4374	0.6532	0.9735	0.2294
BC	0.4027	0.4289	0.5059	0.2798	0.8874	0.1190	0.2309	0.0344
A^2	0.0043	0.0540	0.0637	0.1643	0.2163	0.0112	0.0798	0.1253
B^2	0.0003	< 0.0001	0.0024	0.0005	0.0015	0.0315	0.0002	< 0.0001
C^2	0.0006	< 0.0001	0.0207	0.0013	0.0023	0.0292	0.0002	< 0.0001
Lack of Fit	0.4994	0.2058	0.7622	0.2826	0.0913	0.0607	0.2836	0.6795
R^2	0.9877	0.9866	0.9619	0.9755	0.9509	0.9634	0.9875	0.9905
Adjusted R^2	0.9720	0.9693	0.9129	0.9439	0.8877	0.9163	0.9714	0.9784

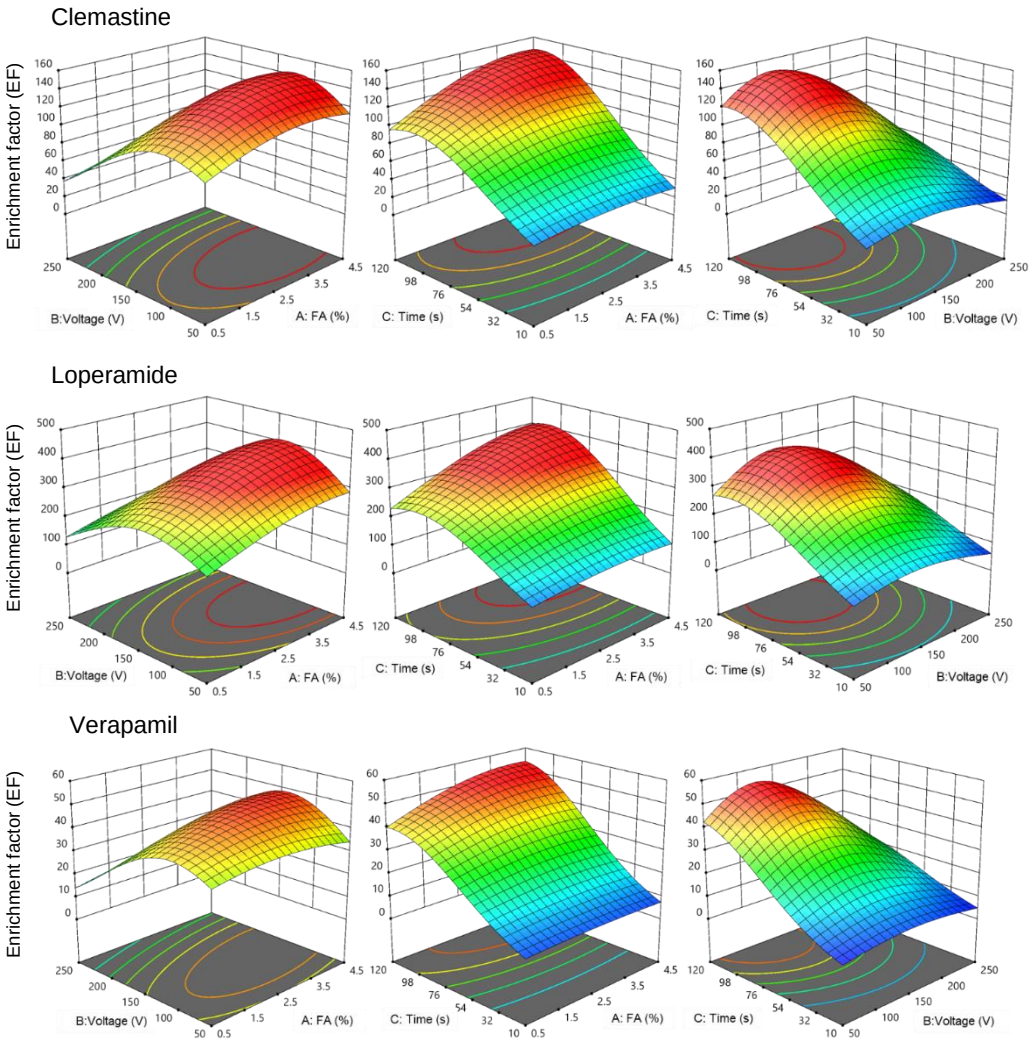

Figure 3. Surface profiles of the developed quadratic models for representative model compounds, *i.e.*, clemastine, loperamide, and verapamil, as a function of extraction voltage and/or FA percentage or electro-extraction time at the optimum parameters.

Under the optimal circumstances, the resulting EF of the academic samples ranges from 20 for propranolol to 387 for loperamide, and it showed a partial positive correlation with the polarity of the compounds, which was also observed in [33]. The low EF of propranolol may be due in part to it being more polar (logP=3.0) than the other analytes (logP=3.7-5.3), which affects solubility and migration through the organic phase [36]. The highest optimal EF of loperamide may be due to its higher lipophilicity (logP=4.4) and larger pKa value (9.4), which improves its charge state and dissolution in the organic phase.

The optimum extraction time of 98 seconds is significantly faster than extraction times of 2.5-33.3 minutes reported in other studies [29, 33, 34, 37-40, 47, 58, 59]. This comparably short extraction time could be the combined contribution of higher extraction voltage, lower volume of the acceptor droplet, and a high surface-area-to-volume ratio of the near-spherical acceptor droplet. In comparison, the achieved EF (20.1-36.8) and recovery of 5.0-9.2% (Table S1) of amitriptyline, propranolol, and oxeladin, are lower than reported in our previous work (EF=104.7-135.7, ER=10-13%) [36]. This may be due to the bigger acceptor droplet (0.5 µL) used here compared to our previous study (0.25 µL) [36], which induced a lower enrichment during extraction, and the simultaneous optimization of the EE method for more model compounds with different polarity and charge status than the previous study, for instance, clemastine, clomipramine, haloperidol, loperamide, and verapamil. The longer extraction time compared to our previous study may be due to the use of more relatively polar and less basic model compounds, *i.e.*, haloperidol and clomipramine, and the simultaneous optimization of the EE method for all of these compounds [36]. Under the optimal extraction conditions, the total time for the extraction is around 4 min, which was shorter compared to our previously-reported manual EE setup [41]. This includes the automated addition of the sample and organic solvent, forming, aspirating, and injecting the acceptor droplet, and finally cleaning the CTC syringe.

3.1.3 Application and performance evaluation

To further investigate the applicability of the automated electro-extraction setup to biological samples, 50 ng mL^{-1} of analytes were spiked into human plasma and urine samples before diluting to 1-fold, 5-fold, and 10-fold of the starting volume. The influence of protein precipitation (PP) on plasma samples and the effect of dilution on the PP samples was also investigated by spiking the model compounds before PP. As shown in Figure 4,

no significant difference in enrichment factor was observed between the undiluted, 5-fold, and 10-fold diluted plasma samples with PP in amitriptyline, haloperidol, oxeladin, and

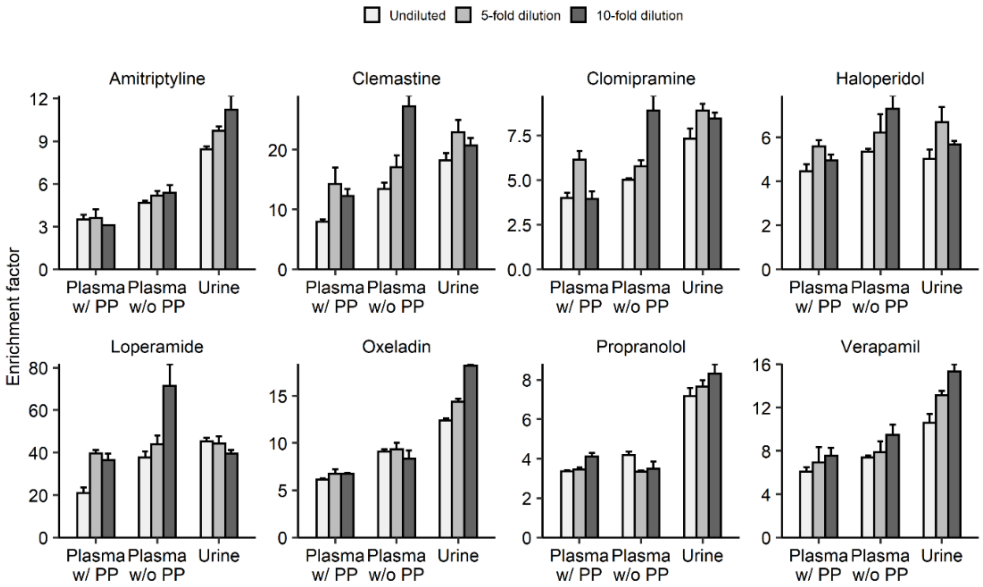

verapamil, suggesting that dilution has limited effect on the extraction performance when the samples are protein precipitated prior to the electro-extraction.

Figure 4. The enrichment factor of model compounds spiked in undiluted, 5-fold and 10-fold diluted plasma, with protein precipitation (w/ PP), without protein precipitation (w/o PP), and urine (n=3).

However, in plasma samples without PP, the enrichment factor notably increased with dilution (Figure 4), and for clemastine, clomipramine, loperamide, and verapamil, the enrichment factor after 10-fold dilution was significantly higher ($p<0.05$) than in undiluted samples. However, the gain in enrichment factor was less than the dilution factor, resulting in an overall dilution of the sample. Plausible causes are that dilution reduced the concentration of the proteins from the plasma presenting at the interface between the sample and the organic phase, which improved the migration of analytes from sample to acceptor droplet [36, 41], and/or less ion suppression induced by the dilution. For all model compounds, the enrichment factor in plasma appeared to be lower after protein precipitation, which may be due to the protein binding of some compounds and loss of analytes during protein precipitation [60-66]. However, it also indicates that the optimized EE method is

able to separate the molecules with high protein affinity from the proteins (in the samples without PP). For the urine sample, the enrichment factor was also notably higher ($p<0.05$) for 10-fold diluted samples than for 5-fold diluted and/or undiluted samples, indicating the reduced ion suppression and/or improved performance of the extraction. The gain in enrichment factor however is small and does not offset the loss due to dilution. The higher enrichment factor of academic samples (Table S1) compared to the enrichment factor of the biological (plasma and urine) samples was consistent with our previous work [36] and indicates that matrix effects occurred during the extraction process in biological samples. Overall, the enrichment factors in plasma and urine samples demonstrate a stable extraction process even with these matrix effects.

The current during electro-extraction of the biological samples was also recorded and shown in Figure 5. A relatively more stable and constant current was measured during the extraction of urine and protein-precipitated plasma compared to the non-precipitated plasma, and the average current level was reduced with an increased dilution factor. This observation is consistent with Equation 3, which describes that low cationic substance concentration in the sample solution (C_{ih}) obtained by dilution induces lower fluxes (J_i), and further results in a lower current (Equation 4).

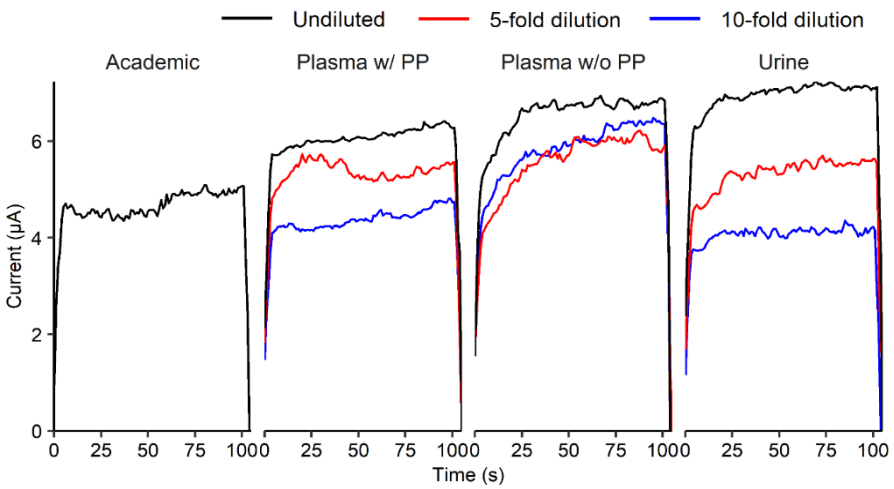

Figure 5. The current monitored by optimal automated EE setup in undiluted, 5-fold, and 10-fold diluted urine, plasma with protein precipitation (w/ PP), plasma without protein precipitation (w/o PP), and academic sample with optimal EE method.

Babu *et al.* observed that higher protein concentration decreased sample conductivity and increased resistance [67], which is positively related to Joule heating. The increasing current in the non-precipitated plasma in Figure 5 may be related to decreased conductivity, increased Joule heating, and increased temperature induced by higher protein concentrations. This is consistent with Gjelstad *et al.*'s theoretical model whereby increased temperature results in increased current during electro-extraction [42]. These current profiles differ from the initial spike in the current as observed with crystal violet (Figure 2), which increased fast and then decreased before stabilizing. This may be the contribution of the different concentration of crystal violet (1000 ng mL^{-1}) and non-optimal EE parameters used in Figure 2. To explore the possible reasons for this difference, various concentrations of crystal violet were used for the current determination under the optimal EE method. The trend of fast increasing and then decreasing current was observed in all concentrations of crystal violet, and this trend increased with concentration (Figure S4). The highest current value was observed in the highest crystal violet concentration (10000 ng/mL), which was consistent with Gjelstad *et al.*'s observation that a high initial analyte concentration in the sample solution strongly influenced the current and raised it to a high level [42]. The different current profile of crystal violet from the model compounds may be due to the easy charge and hydrophilic property of crystal violet.

Finally, the performance of the automated electro-extraction was evaluated by determining the response function, repeatability, limits of detection (LODs), limits of quantification (LOQs), and accuracy using the optimum extraction conditions with a small starting sample volume with 20 µL, *i.e.*, 10-fold diluted urine and plasma. All model compounds exhibited good response function (R^2>0.99) within the concentration range from 10 to 1000 ng mL^{-1} (Table 3). The LODs and LOQs are in the range of 3.2-29.7 pg mL^{-1} and 10.6-99.1 pg mL^{-1}, respectively. The accuracy (75–128%), intra- and inter-day relative standard deviation (RSD) (< 21%), and all the evaluated results demonstrate the stability, sensitivity, and repeatability of the EE method in both diluted plasma and urine samples. The automated extraction method also achieved better RSD and comparable accuracy (<12.8% and 93-128%, respectively) than our earlier manual procedure (<17.8% RSD and 73-107%, respectively) for the same compounds, *i.e.*, amitriptyline, oxeladin, and propranolol, from undiluted plasma and urine samples. This demonstrates that the automated EE setup provides better repeatability compared to the manual EE setup.

Table 3. Calibration curve and precision (RSD) of the model compounds in diluted plasma and urine samples by using the optimized EE method (n=3).

Matrix	Analyte	Linear range (ng/mL)	Response function (R^2)	LOD (S/N=3) (pg/mL)	LOQ (S/N=10) (pg/mL)	Accuracy (%) (25 ng/mL)	RSD (50 ng/mL)	
							Intraday	Interday
Plasma	Amitriptyline	10 - 1000	0.991	6.9	22.9	94	8.9%	1.5%
	Clemastine	10 - 1000	0.997	13.7	45.8	82	15.5%	19.3%
	Clomipramine	10 - 1000	0.995	25.0	83.4	91	5.7%	21.3%
	Haloperidol	10 - 1000	0.991	5.8	19.3	88	9.2%	11.2%
	Loperamide	10 - 1000	0.994	3.2	10.6	98	6.3%	16.7%
	Oxeladin	10 - 1000	0.997	4.9	16.5	109	10.9%	3.1%
	Propranolol	10 - 1000	0.991	7.3	24.2	128	12.5%	10.4%
	Verapamil	10 - 1000	0.995	7.5	25.1	89	1.0%	19.8%
Urine	Amitriptyline	10 - 1000	0.992	5.5	18.5	93	12.8%	11.9%
	Clemastine	10 - 1000	0.997	29.6	98.7	98	12.5%	8.0%
	Clomipramine	10 - 1000	0.990	29.7	99.1	92	10.1%	11.1%
	Haloperidol	10 - 1000	0.990	7.9	26.5	112	14.5%	9.9%
	Loperamide	10 - 1000	0.999	3.8	12.6	75	15.9%	10.3%
	Oxeladin	10 - 1000	0.990	5.8	19.3	119	2.3%	8.5%
	Propranolol	10 - 1000	0.990	7.5	24.9	107	8.2%	3.9%
	Verapamil	10 - 1000	0.990	8.9	29.8	106	9.0%	9.1%

3.2 Phase 2: Evaluation of the 96-well plate EE module for acylcarnitines analysis

The 3-well EE setup with machine vision and current monitoring in section 3.1 demonstrated a robustly-developed EE module. However, the designed well plate holds only three samples for EE. For the start of each new sample, the well plate had to be manually moved to the proper position to align the syringe needle with the sample, which does not provide the required throughput for bioanalysis. Therefore, an in-house developed 96-well plate with an integrated bottom electrode was utilized for human plasma and *Ercc1*$^{\Delta/-}$ mice muscle tissue analysis of acylcarnitines. Firstly, the EE parameters were optimized for simultaneous extraction of ten acylcarnitines from academic samples. Then the optimal EE method was applied to human plasma samples for extraction performance evaluation. Lastly, the evaluated EE method was applied to *Ercc1*$^{\Delta/-}$ mice samples to investigate whether fast sample isolation (after mouse dissection) is necessary for acylcarnitine stability.

3.2.1 Optimization of the high-throughput EE for acylcarnitines analysis

3.2.1.1 Optimization model design and model quality

Box-Behnken design (BBD) was also utilized to optimize the parameters of the EE setup for acylcarnitines analysis. Three crucial parameters, the ratio of FA in the sample to acceptor phase (A), applied voltage (B), and extraction time (C), were also selected for the simultaneous optimization and evaluation of the fully automated and high-throughput EE setup.

Quadratic models were utilized in BBD, and 17 experiments were conducted in triplicate for the optimization. The investigation range for each parameter is listed in Table S2 and S3. The maximum voltage was determined by the acceptor droplet stability using the EE machine vision setup described in section 3.1. 1000 ng mL^{-1} of crystal violet was spiked in the academic sample for this determination to allow the acceptor droplet to be easier visualized by a camera. A long extraction time, 900 seconds, was conducted for the determination based on a previous acylcarnitine electroextraction study [33]. 200 V was set as the highest voltage since it is the maximum voltage the acceptor droplet kept stable for at least 900 s (Figure S5).

The developed quadratic models were all significant ($p<0.02$), and the lack of fit of these models was insignificant ($p>0.06$) for acylcarnitines in the acceptor phase with 2.0% FA (Table S4) and 0.5% FA (Table S5), indicating a good fit of the developed models with the parameters used for acylcarnitine electroextraction optimization. The determination coefficient of the developed models, R^2 (>0.91 and >0.87 for 2.0% FA and 0.5% FA acceptor phase, respectively) and adjusted R^2 (>0.80 and >0.71 for 2.0% FA and 0.5% FA acceptor phase, respectively), also revealed the good fit of models regardless of the acylcarnitine species (Table S4 and S5). Overall, the developed models fit well with the parameters and analytes in the subsequent optimizations.

3.2.1.2 Optimization of the 96-well plate EE setup for acylcarnitines

The ratio of FA in the sample to acceptor phase, extraction voltage, and time are three critical parameters of electro-extraction and were thoroughly investigated. The models for the acceptor phase with 2.0% FA and 0.5% FA were optimized separately. The optimum enrichment factors of acylcarnitines in these two acceptor phases were compared to determine a better ratio of FA in the sample to acceptor droplet for the automated EE method. Table 4 suggested that the optimized EF in the acceptor phase with 2.0% FA was significantly higher compared to that with 0.5% FA. For the acceptor phase with 2.0% FA, the optimum EF of acylcarnitines was obtained at a ratio of FA in the sample to acceptor phase of 1.25 (2.5% FA in sample), extraction voltage of 175 V, and extraction time of 693 s (Figure 6).

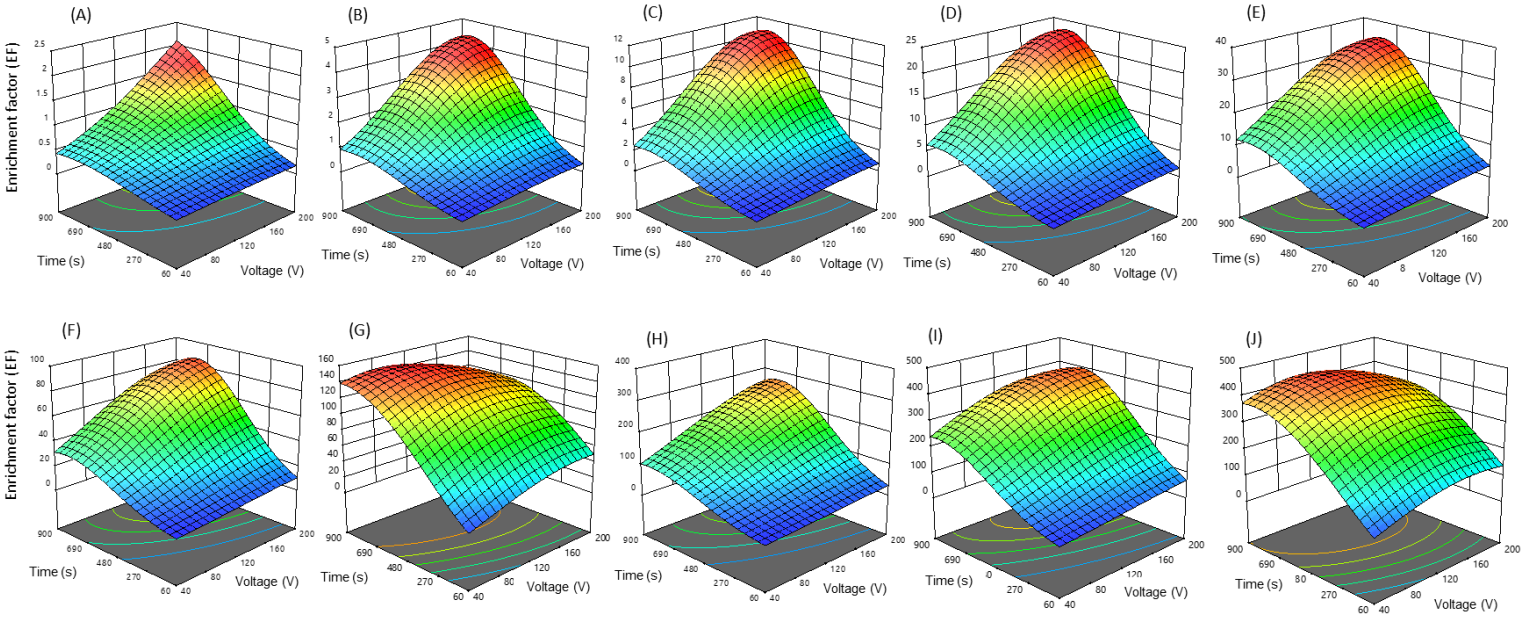

Figure 6. Surface profiles of the developed quadratic models for carnitine (A), acetyl-carnitine (B), propionyl-carnitine (C), isobutyryl-carnitine (D), valeryl-carnitine (E), hexanoyl-carnitine (F), octenoyl-carnitine (G), octanoyl-carnitine (H), decanoyl-carnitine (I), and lauroyl-carnitine (J) as function of electro-extraction time (x-axis) and extraction voltage (y-axis) at the optimum formic acids 2.5% in sample, and 2.0% in acceptor droplet.

Table 4. The optimal EF and ER of acylcarnitines in acceptor droplet with 2.0% and 0.5% of FA.

		Carnitine	Acetyl-carnitine	Propionyl-carnitine	Isobutyryl-carnitine	Valeryl-carnitine
2.0% FA	EF	1.47	3.93	9.99	21.39	33.07
	ER	0.37%	0.98%	2.50%	5.35%	8.27%
0.5% FA	EF	0.68	1.83	4.83	12.46	25.44
	ER	0.17%	0.46%	1.21%	3.12%	6.36%
		Hexanoyl-carnitine	Octenoyl-carnitine	Octanoyl-carnitine	Decanoyl-carnitine	Lauroyl-carnitine
2.0% FA	EF	82.00	130.47	246.49	393.41	397.31
	ER	20.50%	32.62%	61.62%	98.35%	99.33%
0.5% FA	EF	72.16	51.47	164.58	271.63	235.86
	ER	18.04%	12.87%	41.15%	67.91%	58.97%

During electroextraction of acylcarnitines, the acceptor droplet acts as the cathode, where the pH increased with electrolysis, leading to a shift in charge state equilibrium, polarity, and solubility of the acylcarnitines in the aqueous acceptor droplet, which has been reported in previous electro-driven extraction studies [29, 33, 36, 37, 51, 57]. A higher FA percentage in the acceptor phase slows down the pH increase during EE, resulting in less back extraction of acylcarnitines into the organic phase, and higher enrichment factors in the acceptor phase. A higher percentage of FA in aqueous samples contributes to an increased buffer capacity and a more stable pH during EE. However, the EF of acylcarnitines decreased when the FA was greater than its optimum value in the sample, 2.5% (or the FA ratio was larger than 1.25). Similar results of a declining trend in the enrichment factor after FA % (or FA ratio of sample to acceptor phase) reaching the optimum values were also observed by Nojavan *et al.* [52] and in section 3.1 in this chapter. This may be due to the lower electric field, increased electrolysis during electroextraction, and a too-high ion balance (χ in Equation 3) induced by the high ionic concentration in the sample solution at these conditions [40, 51].

Both the migration of charged acylcarnitines during EE and the extraction efficiency can be improved by higher extraction voltage. However, for voltages greater than the optimum value, 175 V, the EF of some acylcarnitines, *i.e.*, acetyl-carnitine, decanoyl-carnitine, lauroyl-carnitine, isobutyryl-carnitine, octenoyl-carnitine, propionyl-carnitine, and valeryl-carnitine, decreased. Similar results of reduced EF at voltages above the optimum value

were also reported by Schoonen *et al.* [54], Nojavan *et al.* [52, 53], and in section 3.1. Simultaneously, the same declining trend of EF was also observed in extraction time after reaching the optimal value, 693 s. These declining EF trends during method optimization may be explained by the excessive electrolysis in the acceptor phase [51, 55-57], the shift charge state, reduced polarity, and increased back extraction of these kinds of acylcarnitines into the organic phase through a passive liquid-liquid extraction, which has been observed in numerous previous studies [29, 33, 36, 37, 51, 57]. This antagonistic effect between extraction time and voltage was also consistent with the theoretical model of analyte flux (J_i) in Equation 3 [50].

The enrichment factor of acylcarnitines was also highly related to their polarities (log P value) (Figure 7). The more polar the analytes, the lower their EF, *i.e.*, carnitine (log P = -4.9, EF = 1.5), acetyl-carnitine (log P = -4.4, EF = 4.0), and propionyl-carnitine (log P = -3.3, EF = 10.0). Decanoyl-carnitine and lauroyl-carnitine reached nearly the maximum EF (400) with the highest log P values, *i.e.*, -0.63 and 0.26, respectively. A similar EF trend with analyte polarity was also observed in Raterink *et al.'s* study [33]. The much higher optimum enrichment factors of some acylcarnitines, *i.e.*, lauroyl-carnitine (397), decanoyl-carnitine (393), octanoyl-carnitine (246), octenoyl-carnitine (130), and hexanoyl-carnitine (82), compared to Raterink *et al.*'s results (< 25) may be due to the contribution of a smaller acceptor droplet (0.5 µL versus 2.0 µL) and a higher optimum extraction voltage (175 V versus 140 V) in our study [33]. The extraction time and recovery were comparable with Raterink *et al.*'s EE method [33].

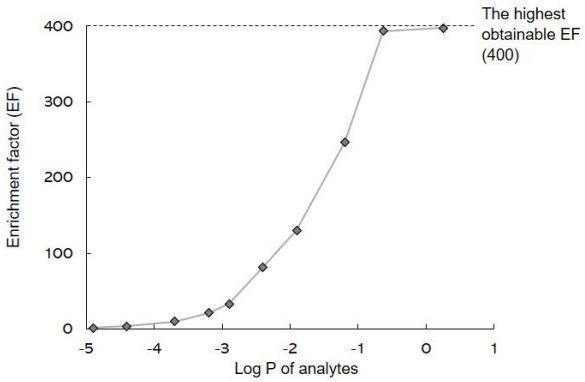

Figure 7. The optimal enrichment factor versus log P of acylcarnitines

3.2.1.3 Application and performance evaluation of the high-throughput EE

To further investigate the optimized and fully-automated EE setup for biological samples, ten acylcarnitine standards were spiked into undiluted, 5-fold diluted, and 10-fold diluted human plasma samples with and without protein precipitation (with 2.5% FA added). Significantly ($p<0.05$) higher EF for some acylcarnitines, *i.e.*, acetyl-carnitine, hexanoyl-carnitine, lauroyl-carnitine, isobutyryl-carnitine, octenoyl-carnitine, propionyl-carnitine, and valeryl-carnitine, were observed in 10-fold (or 5-fold) diluted plasma compared to the undiluted plasma samples without PP, indicating that dilution reduced matrix effects and improved automated EE performance in plasma samples (Figure 8). A plausible reason may be that dilution decreased protein amount from the plasma present at the interface between the sample and organic layer, which reduced the potential protein bands for the analyte's migration from sample to acceptor droplet and improved the extraction efficiency. Similar results were also reported in [36, 41], and observed in section 3.1 for basic compound extraction. For most acylcarnitines, the EF in plasma with PP was notably ($p<0.05$) lower than that in plasma without PP, which may be due to the loss of these analytes during the PP procedure (Figure 8). Even though the EF of acylcarnitines in plasma samples was smaller than in academic samples (Table 4), the values were much larger than in the previous acylcarnitine electroextraction study in plasma [33], demonstrating the improved extraction efficiency of the fully-automated EE setup for acylcarnitines.

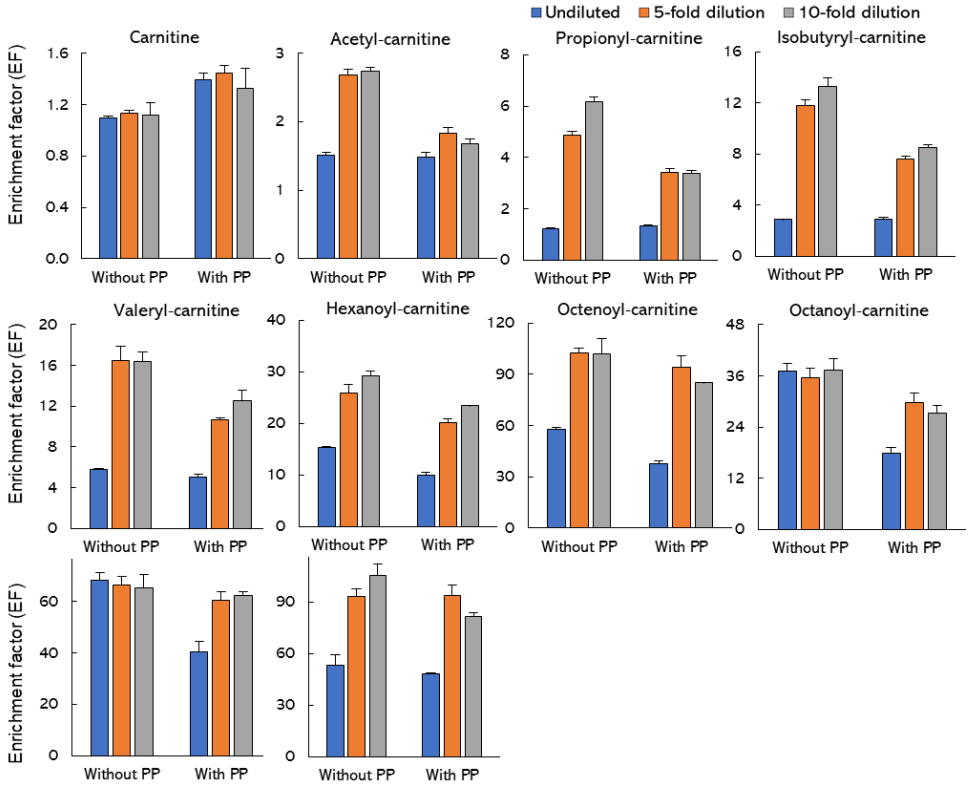

Figure 8. The EF of acylcarnitines spiked in undiluted, 5-fold, and 10-fold diluted plasma samples with and without protein precipitation (PP) (n=3).

The automated EE setup was further characterized by determining the response function, repeatability, limits of detection (LODs), limits of quantification (LOQs), and accuracy before its application in muscle tissues (Table 5). The optimum extraction conditions that yielded the highest enrichment factor, *i.e.*, 10-fold diluted plasma without PP, were utilized for the evaluation. The good response function (R^2>0.99) within the concentration range of 10–1000 ng mL^{-1}, low LODs (<25.8 ng mL^{-1}) and LOQs (82.2 ng mL^{-1}), high accuracy value (88–112%), acceptable intra- and inter-day relative standard deviation (RSD) (<18%) of kinds of acylcarnitines demonstrated the stability, sensitivity, and repeatability of the automated EE setup in plasma samples.

Table 5. Calibration curve and precision (RSD) of the model compounds in diluted plasma samples by using the optimized EE method (n = 3).

Analyte	Linear range (ng/mL)	Response function (R^2)	LODs (ng/mL)	LOQs (ng/mL)	Accuracy (%) (50 ng/mL)	RSD (50 ng/mL)	
						Intraday	Interday
Carnitine	10 - 1000	0.9950	3.9	13.0	102	8.10%	11.51%
Acetyl-carnitine	10 - 1000	0.9904	25.8	85.2	91	2.09%	12.89%
Propionyl-carnitine	10 - 1000	0.9941	6.7	22.1	101	6.18%	10.34%
Lsobutyryl-carnitine	10 - 1000	0.9912	7.8	25.6	102	11.91%	9.66%
Valeryl-carnitine	10 - 1000	0.9905	13.5	44.5	91	17.95%	14.99%
Hexanoyl-carnitine	10 - 1000	0.9901	11.2	37.0	89	16.69%	12.47%
Octenoyl-carnitine	10 - 1000	0.9948	3.0	9.8	112	4.41%	3.75%
Octanoyl-carnitine	10 - 1000	0.9975	6.5	21.5	91	9.97%	16.63%
Decanoyl-carnitine	10 - 1000	0.9960	5.5	18.2	96	5.82%	12.31%
Lauroyl-carnitine	10 - 1000	0.9932	4.2	13.7	107	16.02%	17.12%

The current during electroextraction of biological samples was also recorded, and the results of samples that yielded the highest enrichment factor, *i.e.*, 10-fold diluted plasma is shown in Figure S6B and C. A relatively stable current was observed in academic (Figure S6A) and plasma samples with PP (Figure S6C), which was similar to our observation in section 3.1. Babu *et al.* observed that higher protein concentration increased sample nonconductivity [67]. The increasing current in plasma sample without PP until 200 s in our study may be due to the decreased solvent conductivity, increased Joule heating, and increased temperature induced by higher proteins concentrations, which was consistent with Gjelstad *et al.*'s report that increased temperature results in increased current during electroextraction [42]. A slowly decreasing and stable current after 200 s in plasma sample without PP may be due to the heat exchange between EE solvents and the environment, which results in a slightly decreasing and then stable temperature of the solvents for EE.

3.2.2 The effects of sample isolation speed on acylcarnitines stability

To deduce the effect of sample collection speed on the stability of these acylcarnitines, the concentrations of these acylcarnitines in fast and delayed isolated muscle tissues were determined in three muscle specimens, namely the lower hindlimb muscles gastrocnemius and soleus (Gas + Sol), and extensor digitorum longus + tibialis anterior (EDL + TA), and the upper hindlimb muscle quadriceps (Quadr), which are the most used mouse muscles for

molecular analyses. No significant difference was observed between fast and 15-min delayed isolated Gas + Sol, EDL + TA, and Quadr muscles (Table 6), demonstrating muscle collection speed does not affect the acylcarnitine levels in these three muscle specimens at room temperature. This may be due to the stable properties of these acylcarnitines and/or enzymatic inactivity of the tissue at room temperature [68].

Table 6. The p-value of comparison between sample collection speed (fast and 15-min delayed) and its effect on acylcarnitines stability in different muscle types from progeroid mice (n=3).

	Carnitine	Acetyl-carnitine	Propionyl-carnitine	Isobutyryl-carnitine	Valeryl-carnitine
Gas + Sol	0.5490	0.2031	0.2031	0.2031	0.2031
EDL + TA	0.7140	0.4600	0.6690	0.6710	0.3190
Quadr	0.5067	0.5067	0.5067	0.5067	0.6044
	Hexanoyl-carnitine	Octenoyl-carnitine	Octanoyl-carnitine	Decanoyl-carnitine	Lauroyl-carnitine
Gas + Sol	0.2031	NA	0.2031	0.2031	0.2374
EDL + TA	0.8860	NA	0.3260	0.7270	0.1730
Quadr	0.5067	0.5150	0.5067	0.5150	0.6120

Note: NA means nothing measured.

4. Conclusion

Firstly, three-phase electro-extraction (EE), with machine vision for calculation of acceptor droplet size and current monitoring, was developed in a 3-well plate module integrated on a CTC PAL robotic autosampler and coupled to LC-MS. Eight model compounds, *i.e.* amitriptyline, clemastine, clomipramine, haloperidol, loperamide, propranolol, oxeladin, and verapamil, were utilized for the evaluation of stability and extraction performance of the developed setup. The results proved a stable and repeatable automated EE setup, achieving enrichment factors (EFs) of 20-387 with an optimum extraction time of 98 seconds for academic samples. For application to human urine and plasma samples, the LODs were down to 3.2 pg mL^{-1} from an equivalent of 20 µL of plasma, with a response function of R^2>0.99.

Secondly, a fully automated and high-throughput EE setup was developed by using an in-house developed 96-well plate with an integrated bottom electrode. A Design of Experiment

approach (Box-Behnken design) was utilized for the parameter optimization of acylcarnitine extraction and showed good fitness ($p<0.006$, $R^2>0.91$). The EFs measured by the optimized EE setup ranged from 1.5 to 397.3 for academic samples. The optimized automated high-throughput EE setup was successfully applied to human plasma samples with LODs down to 3.0 ng mL^{-1} and then utilized for an acylcarnitine stability investigation in progeroid (*Ercc1*$^{\Delta/-}$) mice muscle tissues. The results showed that muscle isolation speed did not affect acylcarnitine levels in progeroid mouse muscle tissues.

In summary, this work demonstrates a stable and robust automated and high-throughput electro-extraction platform that can be directly coupled to LC-MS for bioanalysis of large numbers of samples with small volume/mass and low concentration analytes. 4-15 samples can be analyzed per hour based on the time required for the steps during EE procedure, including cleaning the syringe, and preparing for the next sample. We believe that this technique can provide an excellent solution for sample-preparation bottlenecks of large numbers of samples with limited amount and will contribute to future development of fully automated and high-throughput bioanalysis workflows.

Acknowledgments

The authors are grateful to Emiel Wiegers, Raphaël Zwier, and Gijsbert Verdoes from the Fine Mechanical Department (FMD), and Raymond Koehler and Peter van Veldhuizen from the Electronics Department (ELD) at Leiden University for their contribution in developing the hardware and electronics of this setup. We thank Tom Vercammen from Interscience for discussions and suggestions regarding the development and integration of the electro-extraction setup in the CTC PAL3 autosampler. This work was supported by the Netherlands Organisation for Scientific Research (NWO) in the Building Blocks of Life (No. 737.016.015); the China Scholarship Council (CSC) (No. 201706320322); and (partially) funded by X-Omics (NWO, project 184.034.019).

Reference

[1] L.G. Blomberg, Two new techniques for sample preparation in bioanalysis: Microextraction in packed sorbent (MEPS) and use of a bonded monolith as sorbent for sample preparation in polypropylene tips for 96-well plates. Analytical and Bioanalytical Chemistry, (393) 2009. 797-807.

[2] J. Henion, E. Brewer, and G. Rule, Sample preparation for LC/MS/MS: Analyzing biological and environmental samples. Analytical Chemistry, (70) 1998. 650a-656a.

[3] R.N.X. Xu, L.M. Fan, M.J. Rieser, and T.A. El-Shourbagy, Recent advances in high-throughput quantitative bioanalysis by LC-MS/MS. Journal of Pharmaceutical and Biomedical Analysis, (44) 2007. 342-355.

[4] R.J. Raterink, P.W. Lindenburg, R.J. Vreeken, R. Ramautar, and T. Hankemeier, Recent developments in sample-pretreatment techniques for mass spectrometry-based metabolomics. Trac-Trends in Analytical Chemistry, (61) 2014. 157-167.

[5] W.P. Vermeij, J.H. Hoeijmakers, and J. Pothof, Genome Integrity in Aging: Human Syndromes, Mouse Models, and Therapeutic Options. Annu Rev Pharmacol Toxicol, (56) 2016. 427-45.

[6] M.E. Dolle, R.V. Kuiper, M. Roodbergen, J. Robinson, S. de Vlugt, S.W. Wijnhoven, R.B. Beems, L. de la Fonteyne, P. de With, I. van der Pluijm, L.J. Niedernhofer, P. Hasty, J. Vijg, J.H. Hoeijmakers, and H. van Steeg, Broad segmental progeroid changes in short-lived Ercc1(-/Delta7) mice. Pathobiol Aging Age Relat Dis, (1) 2011.

[7] G. Weeda, I. Donker, J. de Wit, H. Morreau, R. Janssens, C.J. Vissers, A. Nigg, H. van Steeg, D. Bootsma, and J.H. Hoeijmakers, Disruption of mouse ERCC1 results in a novel repair syndrome with growth failure, nuclear abnormalities and senescence. Curr Biol, (7) 1997. 427-39.

[8] J.A. Marteijn, H. Lans, W. Vermeulen, and J.H. Hoeijmakers, Understanding nucleotide excision repair and its roles in cancer and ageing. Nature reviews Molecular cell biology, (15) 2014. 465-481.

[9] E.L. de Graaf, W.P. Vermeij, M.C. de Waard, Y. Rijksen, I. van der Pluijm, C.C. Hoogenraad, J.H. Hoeijmakers, A.F. Altelaar, and A.J. Heck, Spatio-temporal analysis of molecular determinants of neuronal degeneration in the aging mouse cerebellum. Mol Cell Proteomics, (12) 2013. 1350-62.

[10] M.J. Yousefzadeh, J. Zhao, C. Bukata, E.A. Wade, S.J. McGowan, L.A. Angelini, M.P. Bank, A.U. Gurkar, C.A. McGuckian, M.F. Calubag, J.I. Kato, C.E. Burd, P.D. Robbins, and L.J. Niedernhofer, Tissue specificity of senescent cell accumulation during physiologic and accelerated aging of mice. Aging Cell, (19) 2020. e13094.

[11] K. Alyodawi, W.P. Vermeij, S. Omairi, O. Kretz, M. Hopkinson, F. Solagna, B. Joch, R.M.C. Brandt, S. Barnhoorn, N. van Vliet, Y. Ridwan, J. Essers, R. Mitchell, T. Morash, A. Pasternack, O. Ritvos, A. Matsakas, H. Collins-Hooper, T.B. Huber, J.H.J. Hoeijmakers, and K. Patel, Compression of morbidity in a progeroid mouse model through the attenuation of myostatin/activin signalling. J Cachexia Sarcopenia Muscle, (10) 2019. 662-686.

[12] W.P. Vermeij, M.E.T. Dollé, E. Reiling, D. Jaarsma, C. Payan-Gomez, C.R. Bombardieri, H. Wu, A.J.M. Roks, S.M. Botter, B.C. van der Eerden, S.A. Youssef, R.V. Kuiper, B. Nagarajah, C.T. van Oostrom, R.M.C. Brandt, S. Barnhoorn, S. Imholz, J.L.A. Pennings, A. de Bruin, Á. Gyenis, J. Pothof, J. Vijg, H. van Steeg, and J.H.J. Hoeijmakers, Restricted diet delays accelerated ageing and genomic stress in DNA-repair-deficient mice. Nature, (537) 2016. 427-431.

[13] L.J. Niedernhofer, G.A. Garinis, A. Raams, A.S. Lalai, A.R. Robinson, E. Appeldoorn, H. Odijk, R. Oostendorp, A. Ahmad, and W. Van Leeuwen, A new progeroid syndrome reveals that genotoxic stress suppresses the somatotroph axis. Nature, (444) 2006. 1038-1043.

[14] I. van der Pluijm, G.A. Garinis, R.M. Brandt, T.G. Gorgels, S.W. Wijnhoven, K.E. Diderich, J. de Wit, J.R. Mitchell, C. van Oostrom, R. Beems, L.J. Niedernhofer, S. Velasco, E.C. Friedberg, K. Tanaka, H. van Steeg, J.H. Hoeijmakers, and G.T. van der Horst, Impaired genome maintenance suppresses the growth hormone--insulin-like growth factor 1 axis in mice with Cockayne syndrome. PLoS Biol, (5) 2007. e2.

[15] B. Schumacher, I. van der Pluijm, M.J. Moorhouse, T. Kosteas, A.R. Robinson, Y. Suh, T.M. Breit, H. van Steeg, L.J. Niedernhofer, W. van Ijcken, A. Bartke, S.R. Spindler, J.H. Hoeijmakers, G.T. van der Horst, and G.A. Garinis, Delayed and accelerated aging share common longevity assurance mechanisms. PLoS Genet, (4) 2008. e1000161.
[16] S. Mitra, Sample Preparation Techniques in Analytical Chemistry. J. Am. Chem. Soc. 126, 5 (2004) 1585-1585.
[17] B. Bojko, K. Gorynski, G.A. Gomez-Rios, J.M. Knaak, T. Machuca, V.N. Spetzler, E. Cudjoe, M. Hsin, M. Cypel, M. Selzner, M.Y. Liu, S. Keshavjee, and J. Pawliszyn, Solid phase microextraction fills the gap in tissue sampling protocols. Analytica Chimica Acta, (803) 2013. 75-81.
[18] M.A. Dineva, L. Mahilum-Tapay, and H. Lee, Sample preparation: a challenge in the development of point-of-care nucleic acidbased assays for resource-limited settings. Analyst, (132) 2007. 1193-1199.
[19] S.X. Peng, M. Cousineau, S.J. Juzwin, and D.M. Ritchie, A 96-well screen filter plate for high-throughput biological sample preparation and LC-MS/MS analysis. Analytical Chemistry, (78) 2006. 343-348.
[20] D. Vuckovic, Current trends and challenges in sample preparation for global metabolomics using liquid chromatography-mass spectrometry. Analytical and Bioanalytical Chemistry, (403) 2012. 1523-1548.
[21] N. Drouin, S. Rudaz, and J. Schappler, Sample preparation for polar metabolites in bioanalysis. Analyst, (143) 2018. 16-20.
[22] P. Miggiels, B. Wouters, G.J.P. van Westen, A.C. Dubbelman, and T. Hankemeier, Novel technologies for metabolomics: More for less. Trac-Trends in Analytical Chemistry, (120) 2019.
[23] I. Kohler, J. Schappler, and S. Rudaz, Microextraction techniques combined with capillary electrophoresis in bioanalysis. Analytical and Bioanalytical Chemistry, (405) 2013. 125-141.
[24] R. Pero-Gascon, F. Benavente, C. Neusüß, and V. Sanz-Nebot, Evaluation of on-line solid-phase extraction capillary electrophoresis–mass spectrometry with a nanoliter valve for the analysis of peptide biomarkers. Analytica Chimica Acta, (1140) 2020. 1-9.
[25] A. Oedit, B. Duivelshof, P.W. Lindenburg, and T. Hankemeier, Integration of three-phase microelectroextraction sample preparation into capillary electrophoresis. Journal of Chromatography A, (1610) 2020. 460570.
[26] A. Sarafraz-Yazdi and A. Amiri, Liquid-phase microextraction. Trac-Trends in Analytical Chemistry, (29) 2010. 1-14.
[27] D.E. Raynie, Modern Extraction Techniques. Analytical Chemistry, (82) 2010. 4911-4916.
[28] Y.Y. Wen, L. Chen, J.H. Li, D.Y. Liu, and L.X. Chen, Recent advances in solid-phase sorbents for sample preparation prior to chromatographic analysis. Trac-Trends in Analytical Chemistry, (59) 2014. 26-41.
[29] A.Y. Song and J. Yang, Efficient determination of amphetamine and methylamphetamine in human urine using electro-enhanced single-drop microextraction with in-drop derivatization and gas chromatography. Analytica Chimica Acta, (1045) 2019. 162-168.
[30] A. Oedit, R. Ramautar, T. Hankemeier, and P.W. Lindenburg, Electroextraction and electromembrane extraction: Advances in hyphenation to analytical techniques. Electrophoresis, (37) 2016. 1170-86.
[31] P.W. Lindenburg, R. Ramautar, and T. Hankemeier, The potential of electrophoretic sample pretreatment techniques and new instrumentation for bioanalysis, with a focus on peptidomics and metabolomics. Bioanalysis, (5) 2013. 2785-2801.
[32] N. Drouin, P. Kuban, S. Rudaz, S. Pedersen-Bjergaard, and J. Schappler, Electromembrane extraction: Overview of the last decade. Trac-Trends in Analytical Chemistry, (113) 2019. 357-363.
[33] R.J. Raterink, P.W. Lindenburg, R.J. Vreeken, and T. Hankemeier, Three-phase electroextraction: a new (online) sample purification and enrichment method for bioanalysis. Anal Chem, (85) 2013. 7762-8.

[34] N. Drouin, J.F. Mandscheff, S. Rudaz, and J. Schappler, Development of a New Extraction Device Based on Parallel-Electromembrane Extraction. Analytical Chemistry, (89) 2017. 6346-6350.
[35] F.A. Hansen, E. Santigosa-Murillo, M. Ramos-Payan, M. Munoz, E.L. Oiestad, and S. Pedersen-Bjergaard, Electromembrane extraction using deep eutectic solvents as the liquid membrane. Analytica Chimica Acta, (1143) 2021. 109-116.
[36] Y. He, P. Miggiels, B. Wouters, N. Drouin, F. Guled, T. Hankemeier, and P.W. Lindenburg, A high-throughput, ultrafast, and online three-phase electro-extraction method for analysis of trace level pharmaceuticals. Analytica Chimica Acta, (1149) 2021.
[37] L.E.E. Eibak, A. Gjelstad, K.E. Rasmussen, and S. Pedersen-Bjergaard, Kinetic electro membrane extraction under stagnant conditions-Fast isolation of drugs from untreated human plasma. Journal of Chromatography A, (1217) 2010. 5050-5056.
[38] L. Xu, P.C. Hauser, and H.K. Lee, Electro membrane isolation of nerve agent degradation products across a supported liquid membrane followed by capillary electrophoresis with contactless conductivity detection. Journal of Chromatography A, (1214) 2008. 17-22.
[39] L. Arjomandi-Behzad, Y. Yamini, and M. Rezazadeh, Extraction of pyridine derivatives from human urine using electromembrane extraction coupled to dispersive liquid-liquid microextraction followed by gas chromatography determination. Talanta, (126) 2014. 73-81.
[40] A. Slampova, P. Kuban, and P. Bocek, Quantitative aspects of electrolysis in electromembrane extractions of acidic and basic analytes. Analytica Chimica Acta, (887) 2015. 92-100.
[41] Y. He, N. Drouin, B. Wouters, P. Miggiels, T. Hankemeier, and P.W. Lindenburg, Development of a fast, online three-phase electroextraction hyphenated to fast liquid chromatography–mass spectrometry for analysis of trace-level acid pharmaceuticals in plasma. Analytica Chimica Acta, (1192) 2022. 339364.
[42] A. Gjelstad, K.E. Rasmussen, and S. Pedersen-Bjergaard, Simulation of flux during electro-membrane extraction based on the Nernst-Planck equation. Journal of Chromatography A, (1174) 2007. 104-111.
[43] T.M. Middelthon-Bruer, A. Gjelstad, K.E. Rasmussen, and S. Pedersen-Bjergaard, Parameters affecting electro membrane extraction of basic drugs. Journal of Separation Science, (31) 2008. 753-759.
[44] Y. Yang, C. Cruickshank, M. Armstrong, S. Mahaffey, R. Reisdorph, and N. Reisdorph, New sample preparation approach for mass spectrometry-based profiling of plasma results in improved coverage of metabolome. J Chromatogr A, (1300) 2013. 217-26.
[45] V. Shinin, B. Gayraud-Morel, and S. Tajbakhsh, Template DNA-strand co-segregation and asymmetric cell division in skeletal muscle stem cells. Methods Mol Biol, (482) 2009. 295-317.
[46] R.D.A.M. Alves, A.D. Dane, A. Harms, K. Strassburg, R.M. Seifar, L.B. Verdijk, S. Kersten, R. Berger, T. Hankemeier, and R.J. Vreeken, Global profiling of the muscle metabolome: method optimization, validation and application to determine exercise-induced metabolic effects. Metabolomics, (11) 2014. 271-285.
[47] N. Drouin, S. Rudaz, and J. Schappler, Dynamic-Electromembrane Extraction: A Technical Development for the Extraction of Neuropeptides. Analytical Chemistry, (88) 2016. 5308-5315.
[48] D.R. Mani, S.E. Abbatiello, and S.A. Carr, Statistical characterization of multiple-reaction monitoring mass spectrometry (MRM-MS) assays for quantitative proteomics. BMC bioinformatics, (13 Suppl 16) 2012. S9-S9.
[49] M. Abdi, M. Balagabri, H. Karimi, H. Hossini, and S.O. Rastegar, Degradation of crystal violet (CV) from aqueous solutions using ozone, peroxone, electroperoxone, and electrolysis processes: a comparison study. Applied Water Science, (10) 2020. 168.
[50] S. Seidi, Y. Yamini, and M. Rezazadeh, Electrically enhanced microextraction for highly selective transport of three β-blocker drugs. Journal of Pharmaceutical and Biomedical Analysis, (56) 2011. 859-866.
[51] K.S. Hasheminasab, A.R. Fakhari, A. Shahsavani, and H. Ahmar, A new method for the enhancement of electromembrane extraction efficiency using carbon nanotube reinforced hollow

fiber for the determination of acidic drugs in spiked plasma, urine, breast milk and wastewater samples. Journal of Chromatography A, (1285) 2013. 1-6.
[52] S. Nojavan, A. Pourahadi, S.S. Hosseiny Davarani, A. Morteza-Najarian, and M. Beigzadeh Abbassi, Electromembrane extraction of zwitterionic compounds as acid or base: Comparison of extraction behavior at acidic and basic pHs. Analytica Chimica Acta, (745) 2012. 45-52.
[53] S. Nojavan and S. Asadi, Electromembrane extraction using two separate cells: a new design for simultaneous extraction of acidic and basic compounds. Electrophoresis, (37) 2016. 587-594.
[54] J.W. Schoonen, V. van Duinen, A. Oedit, P. Vulto, T. Hankemeier, and P.W. Lindenburg, Continuous-Flow Microelectroextraction for Enrichment of Low Abundant Compounds. Analytical Chemistry, (86) 2014. 8048-8056.
[55] C.X. Huang, A. Gjelstad, and S. Pedersen-Bjergaard, Electromembrane extraction with alkylated phosphites and phosphates as supported liquid membranes. Journal of Membrane Science, (526) 2017. 18-24.
[56] C.X. Huang, K.F. Seip, A. Gjelstad, and S. Pedersen-Bjergaard, Electromembrane extraction of polar basic drugs from plasma with pure bis(2-ethylhexyl) phosphite as supported liquid membrane. Analytica Chimica Acta, (934) 2016. 80-87.
[57] M. Balchen, A. Gjelstad, K.E. Rasmussen, and S. Pedersen-Bjergaard, Electrokinetic migration of acidic drugs across a supported liquid membrane. J Chromatogr A, (1152) 2007. 220-5.
[58] A. Wuethrich, P.R. Haddad, and J.P. Quirino, Off-line sample preparation by electrophoretic concentration using a micropipette and hydrogel. Journal of Chromatography A, (1369) 2014. 186-190.
[59] L. Arjomandi-Behzad, Y. Yamini, and M. Rezazadeh, Pulsed electromembrane method for simultaneous extraction of drugs with different properties. Analytical Biochemistry, (438) 2013. 136-143.
[60] M.A. Levitt, J.B. Sullivan, Jr., S.M. Owens, L. Burnham, and P.R. Finley, Amitriptyline plasma protein binding: effect of plasma pH and relevance to clinical overdose. Am J Emerg Med, (4) 1986. 121-5.
[61] H. Hansson, K. Bergvall, U. Bondesson, M. Hedeland, and K. Torneke, Clinical pharmacology of clemastine in healthy dogs. Veterinary Dermatology, (15) 2004. 152-158.
[62] A.E. Balantgorgia, M. Gexfabry, and L.P. Balant, Clinical Pharmacokinetics of Clomipramine. Clinical Pharmacokinetics, (20) 1991. 447-462.
[63] P. Morselli, G. Tedeschi, G. Bianchetti, J. Henry, and R. Braithwaite, *Plasma protein binding of haloperidol: influence of age and disease states*, in *Clinical Pharmacology in Psychiatry*. 1981, Springer. p. 191-196.
[64] K. Sadrjavadi, F. Rahmati, F. Jafari, S. Moradi, A. Nowroozi, and M. Shahlaei, A study on the binding of loperamide to human serum albumin using combination of computational and experimental methods. Biochem Anal Biochem, (6) 2017. 2161-1009.1000346.
[65] W.R. Ravis, D.L. Parsons, and S.J. Wang, Buffer and pH Effects on Propranolol Binding by Human Albumin and α1-Acid Glycoprotein. Journal of Pharmacy and Pharmacology, (40) 2011. 459-463.
[66] D.L. Keefe, Y.G. Yee, and R.E. Kates, Verapamil protein binding in patients and in normal subjects. Clin Pharmacol Ther, (29) 1981. 21-6.
[67] K.S. Babu and J.K. Amamcharla, Rehydration characteristics of milk protein concentrate powders monitored by electrical resistance tomography. JDS Communications, (2) 2021. 313-318.
[68] Y. Zhang, H. Jiang, and P. Hutson, Stability of acetyl-1-carnitine in 5% dextrose using a high-performance liquid chromatography-mass spectrometry times 2 method. Int J Pharm Compd, (16) 2012. 170-3.

Supplementary Information

Table S1. The optimal EF and recovery of the model compounds in academic samples.

	Amitriptyline	Clemastine	Clomipramine	Haloperidol
EF	27.44	141.98	36.53	32.46
Recovery (%)	6.86%	35.50%	9.13%	8.12%
	Loperamide	Oxeladin	Propranolol	Verapamil
EF	387.49	36.83	20.08	49.00
Recovery (%)	96.87%	9.21%	5.02%	12.25%

Table S2. Investigated parameters for Box-Behnken design for 2.0% FA in the acceptor phase.

Code level	A: FA% or ratio of FA in the sample to acceptor phase (2% FA in acceptor phase)	B: Voltage (V)	C: Extraction time (s)
-1	0.2% (0.1)	40	60
0	2.0% (1.0)	120	480
1	3.8% (1.9)	200	900

Note: Code −1, 0, and 1 were used to represent low, middle, and high levels of parameters.

Table S3. Investigated parameters for Box-Behnken design for 0.5% of FA in the acceptor phase.

Code level	A: FA% or ratio of FA in the sample to acceptor phase (0.5% FA in acceptor phase)	B: Voltage (V)	C: Extraction time (s)
-1	0.2% (0.4)	40	60
0	2.0% (4.0)	120	480
1	3.8% (7.9)	200	900

Note: Code −1, 0, and 1 were used to represent low, middle, and high levels of parameters.

Table S4. p-values and R^2 of response surface quadratic models for EF of acylcarnitines with 2% of FA in the acceptor droplet.

Source	Carnitine	Acetyl-carnitine	Propionyl-carnitine	Isobutyryl-carnitine	Valeryl-carnitine	Hexanoyl-carnitine	Octenoyl-carnitine	Octanoyl-carnitine	Decanoyl-carnitine	Lauroyl-carnitine
Model	0.0009	< 0.0001	< 0.0001	< 0.0001	< 0.0001	< 0.0001	0.0031	0.0007	0.0018	0.0056
A: FA	0.8510	0.7197	0.3104	0.5984	0.9019	0.6349	0.3338	0.9049	0.7898	0.8238
B: Voltage	0.0022	< 0.0001	< 0.0001	< 0.0001	< 0.0001	0.0003	0.7475	0.0035	0.0176	0.6742
C: Time	< 0.0001	< 0.0001	< 0.0001	< 0.0001	< 0.0001	< 0.0001	0.0001	< 0.0001	< 0.0001	0.0002
AB	0.7008	0.2321	0.0290	0.0551	0.1902	0.2507	0.1607	0.3422	0.5719	0.2499
AC	0.3634	0.8147	0.4062	0.4857	0.3981	0.4703	0.8575	0.7241	0.8490	0.5604
BC	0.1018	0.2864	0.7659	0.8196	0.5086	0.3288	0.0529	0.6153	0.2876	0.2435
A^2	0.3599	0.1879	0.0374	0.0530	0.1527	0.3324	0.1216	0.3183	0.5661	0.1001
B^2	0.3383	0.0009	0.0004	0.0027	0.0197	0.0710	0.1016	0.2966	0.3189	0.0826
C^2	0.0096	< 0.0001	< 0.0001	< 0.0001	< 0.0001	0.0002	0.0054	0.0030	0.0045	0.0090
Lack of Fit	0.0558	0.4166	0.2945	0.0841	0.0670	0.1367	0.3155	0.6063	0.4628	0.1868
R^2	0.9508	0.9919	0.9946	0.9920	0.9858	0.9791	0.9276	0.9538	0.9384	0.9134
Adjusted R^2	0.8875	0.9814	0.9876	0.9817	0.9674	0.9522	0.8346	0.8944	0.8593	0.8020

Table S5. p-values and R^2 of response surface quadratic models for EF of acylcarnitines with 0.5% of FA in the acceptor droplet.

	Carnitine	Acetyl-carnitine	Propionyl-carnitine	Isobutyryl-carnitine	Valeryl-carnitine	Hexanoyl-carnitine	Octenoyl-carnitine	Octanoyl-carnitine	Decanoyl-carnitine	Lauroyl-carnitine
Model	0.0017	< 0.0001	< 0.0001	< 0.0001	< 0.0001	< 0.0001	0.0070	0.0009	0.0196	0.0069
A: FA	0.2684	0.7612	0.8828	0.6097	0.5502	0.7179	0.3087	0.7275	0.6351	0.1108
B: Voltage	0.0051	< 0.0001	< 0.0001	< 0.0001	< 0.0001	< 0.0001	0.0674	0.0154	0.3546	0.4058
C: Time	< 0.0001	< 0.0001	< 0.0001	< 0.0001	< 0.0001	< 0.0001	0.0017	< 0.0001	0.0017	0.0004
AB	0.9292	0.8804	0.9932	0.9719	0.8312	0.7221	0.1210	0.9354	0.7093	0.2036
AC	0.7909	0.1065	0.0691	0.0360	0.0406	0.1372	0.4663	0.4430	0.6462	0.2817
BC	0.9288	0.1913	0.0472	0.0033	0.0003	0.0009	0.0239	0.0767	0.1682	0.0673
A^2	0.3160	0.5372	0.3918	0.1842	0.0210	0.0643	0.5962	0.3328	0.3675	0.0730
B^2	0.1570	0.0878	0.0303	0.0069	0.0011	0.0065	0.0903	0.1873	0.6845	0.9505
C^2	0.0093	< 0.0001	< 0.0001	< 0.0001	< 0.0001	< 0.0001	0.0020	0.0008	0.0043	0.0112
Lack of Fit	0.2036	0.5295	0.4392	0.3215	0.1857	0.1215	0.0982	0.3522	0.2391	0.0616
R^2	0.9401	0.9817	0.9894	0.9946	0.9960	0.9918	0.9072	0.9500	0.8717	0.9077
Adjusted R^2	0.8631	0.9582	0.9758	0.9875	0.9909	0.9814	0.7879	0.8857	0.7067	0.7891

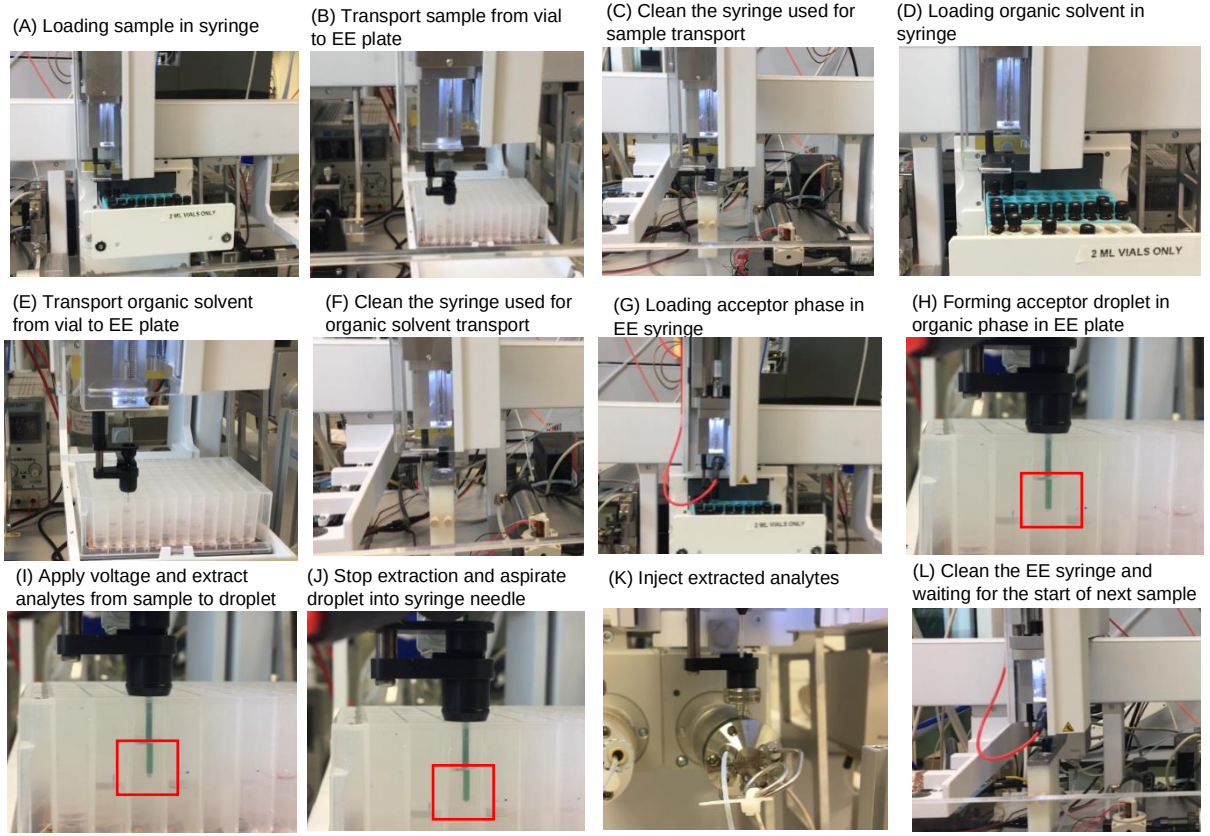

Figure S1. A representative process of the fully automated and high-throughput EE by using crystal violet as sample.

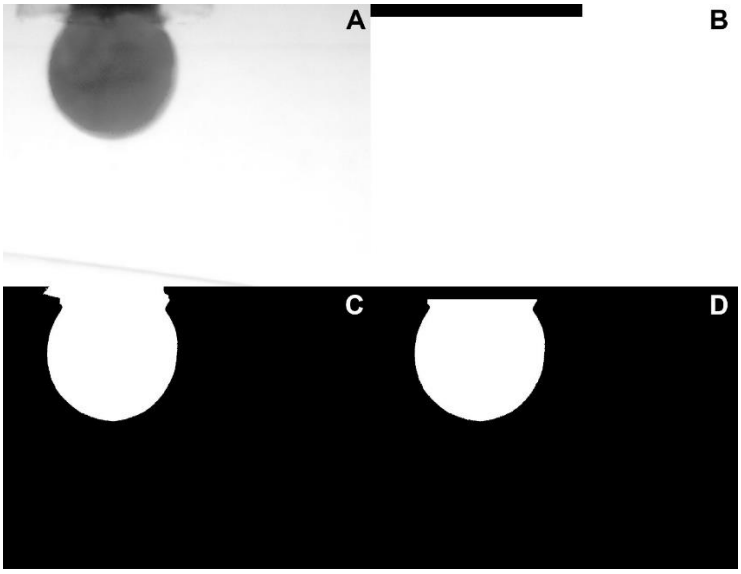

Figure S2. Example of the volume-calculation algorithm using an extracted frame (t=25.0s) from the extraction of crystal violet (2.5% formic acid) at 250V. A) Original frame; B) binarized image of the selected needle region; C) binarized image after thresholding and hole filling; D) binarized image after needle removal, hole filling, and particle removal. Volume was calculated from the final binary image (D) using $V_{droplet} = \frac{\pi}{4} d_{px}^3 \sum_{i=1}^{n} \sum_{j=1}^{n} x_{i,j}^2$, with $d_{px} = 2.25$ µm.

Amitriptyline

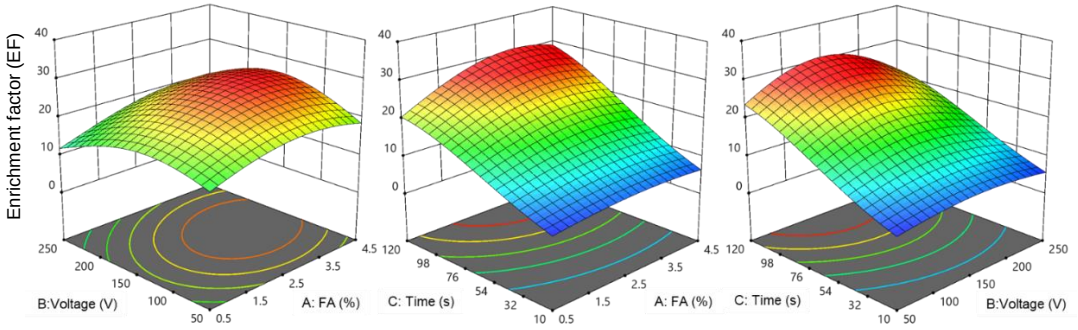

Clomipramine

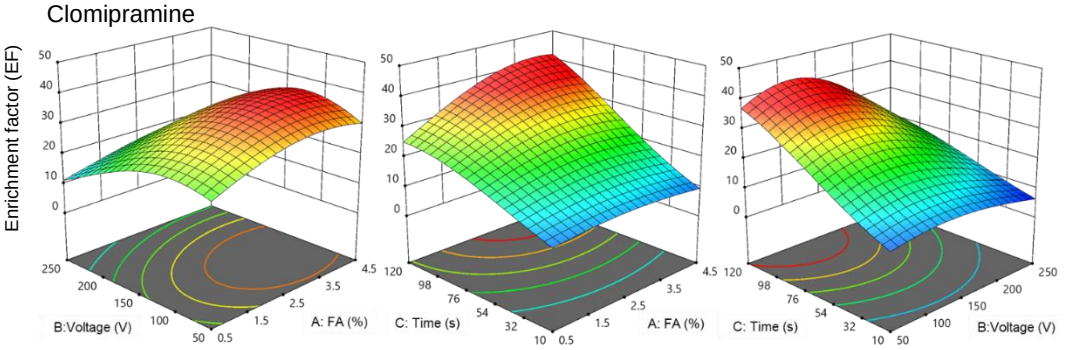

Haloperidol

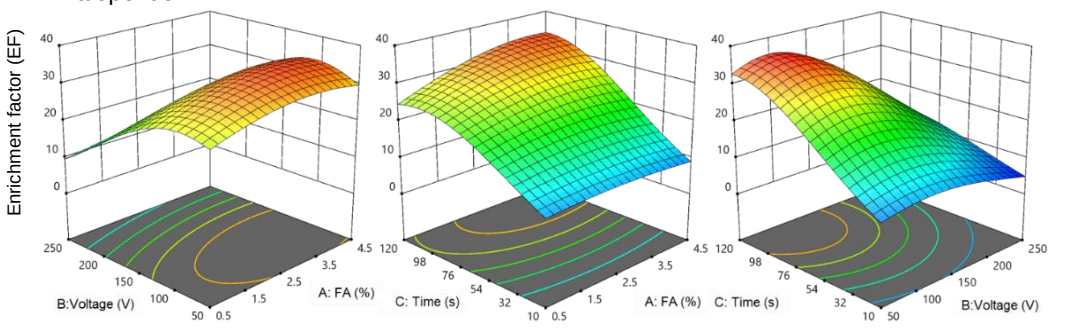

Oxeladin

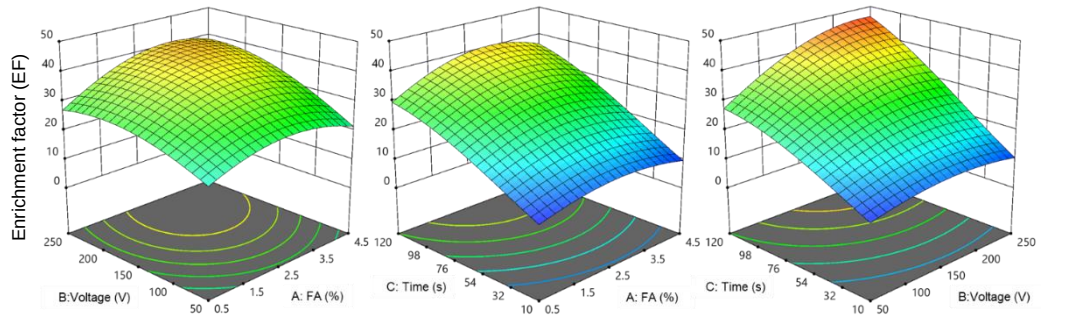

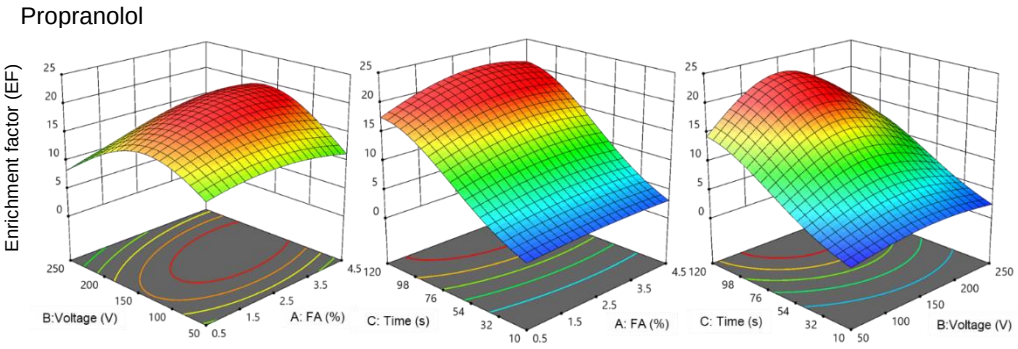

Figure S3. Surface profiles of the developed quadratic models for representative model compounds, *i.e.*, amitriptyline, clomipramine, haloperidol, oxeladin, and propranolol, as a function of extraction voltage and/or FA percentage or electro-extraction time at the optimum parameters.

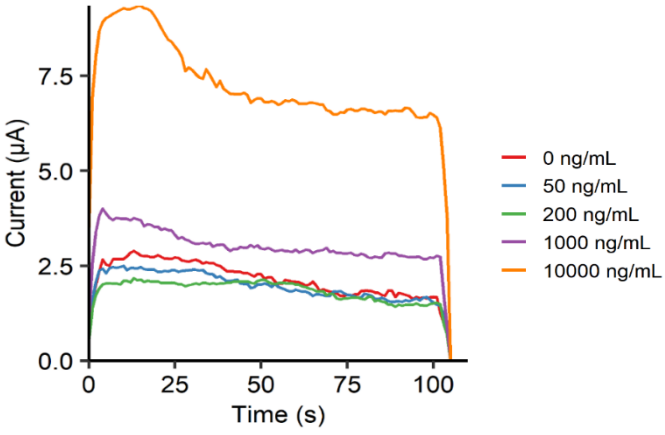

Figure S4. Current profiles of different concentrations of crystal violet (CV) under optimal EE method.

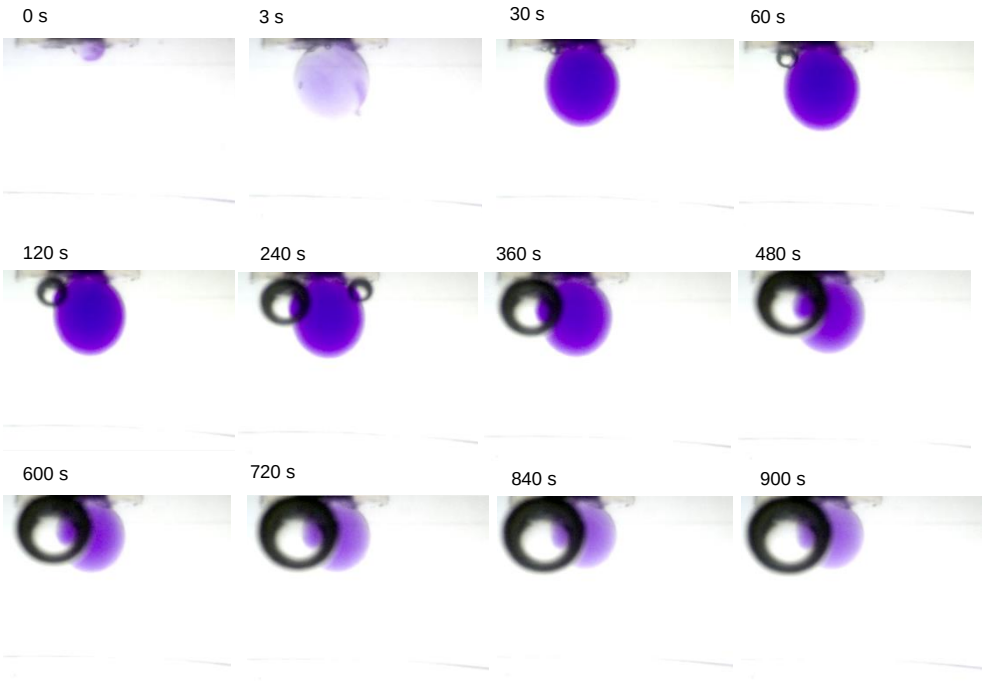

Figure S5. A representative of acceptor droplet stability by using crystal violet and 200 V.

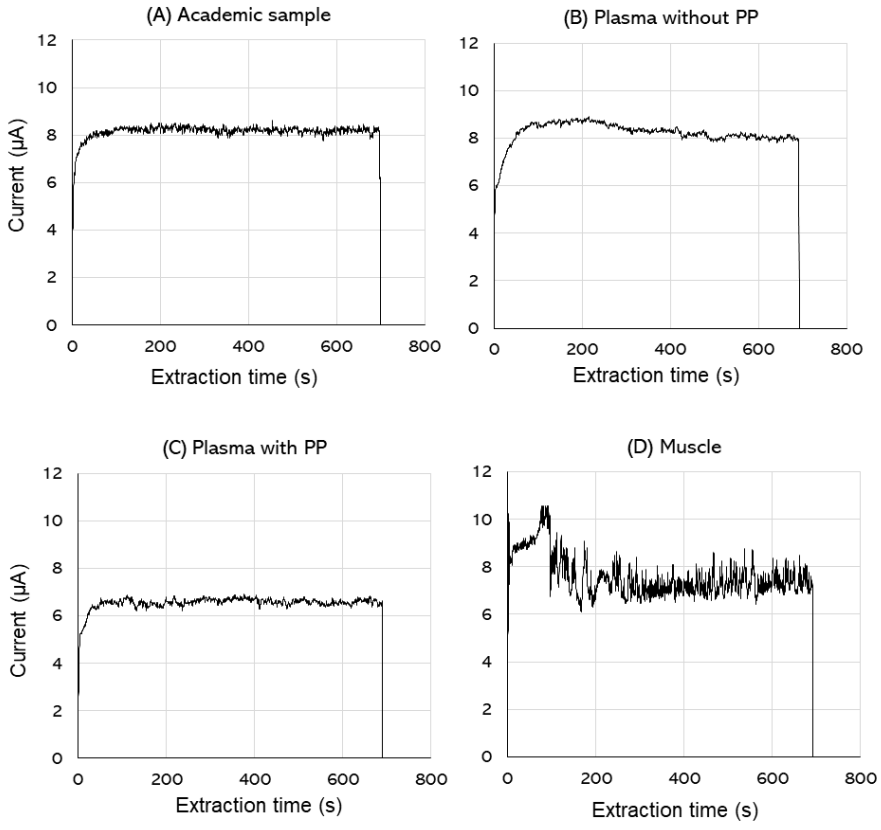

Figure S6. Representatives of the current monitored by automated EE setup in academic samples (A), 10-fold diluted plasma samples without (B) and with (C) protein precipitation (PP), and muscle tissue (D).